MASTER

UCRL-84515
PREPRINT

INELASTIC PROCESSES IN SEISMIC WAVE GENERATION BY UNDERGROUND EXPLOSIONS

Howard C. Rodean
University of California
Lawrence Livermore National Laboratory

This paper was prepared for publication
in the proceedings of the
NATO ADVANCED STUDY INSTITUTE
Identification of Seismic Sources--
Earthquake or Underground Explosion
8-18 September 1980
Oslo, Norway

August 1, 1980

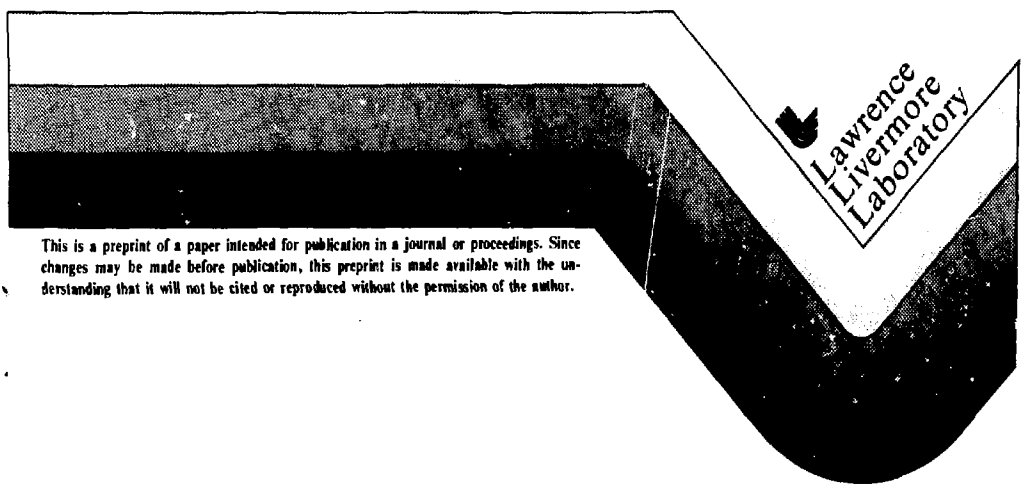

INELASTIC PROCESSES IN SEISMIC WAVE GENERATION BY UNDERGROUND EXPLOSIONS

Howard C. Rodean

University of California
Lawrence Livermore National Laboratory

ABSTRACT

There are similarities and differences between chemical and nuclear explosions underground. Most of the differences are in the early stages of the explosions. The later stages are similar with respect to seismic wave generation. Three sources of seismic waves from explosions are coincident in space and time, or nearly so: the explosion itself, explosion-induced tectonic strain release, and (probably) spall-closure following explosion-produced spall. Cavity collapse and explosion-induced aftershocks are two sources of delayed seismic signals. Theories, computer calculations, and measurements of spherical stress waves from explosions are described and compared, with emphasis on the transition from inelastic to *almost*-elastic relations between stress and strain. Two aspects of nonspherical explosion geometry are considered: tectonic strain release and surface spall. Tectonic strain release affects the generation of surface waves; spall closure may also. The forward problem in seismology can, in principle, be solved by calculations beginning with explosive detonation and ending with the synthetic seismogram. The inverse problem can also, in principle, be solved by inverting observed seismic data to obtain an "equivalent elastic source," but the solution cannot extend backward in space and time into the nonlinear inelastic processes of the explosion. The reduced-displacement potential is a common solution (the "equivalent elastic source") of the forward and inverse problems, assuming a spherical source. Measured reduced-displacement potentials are compared with potentials calculated as solutions of the direct and inverse problems; there are significant differences between the results of the two types of calculations and between calculations and measurements. The simple

spherical model of an explosion is not sufficient to account for observations of explosions over wide ranges of depth and yield. The explosion environment can have a large effect on explosion detection and yield estimation. The best sets of seismic observations for use in developing discrimination techniques are for high-magnitude high-yield explosions; the identification problem is most difficult for low-magnitude low-yield explosions. Most of the presently available explosion data (time, medium, depth, yield, etc.) are for explosions in a few media at the Nevada Test Site; some key questions concerning magnitude vs yield and m_b vs M_S relations can be answered only by data for explosions in other media at other locations.

1. INTRODUCTION

This Advanced Study Institute is concerned with the means for answering the question, "Do the characteristics of a set of observed seismic signals indicate that the source of those signals was an earthquake or an underground explosion?" The subject of this lecture is the inelastic processes that are involved in the generation of seismic waves by underground explosions. The emphasis is on how these inelastic processes determine (or may determine) seismic signal characteristics that are pertinent to seismic identification and two other important aspects of seismic monitoring: event detection and (if the event is identified as an explosion) yield estimation.

The parenthetical phrase, "or may determine," indicates that our knowledge of these inelastic processes is imperfect and incomplete. In this lecture, we will try to distinguish between proven knowledge and informed speculation, and to establish what is known about this subject.

2. PHENOMENA IN CHEMICAL AND NUCLEAR EXPLOSIONS

In the context of this Institute, we may define an underground explosion as a sudden release of concentrated energy, the response of the surrounding rock to this energy, and the consequent radiation of seismic waves. Two sources of concentrated energy are chemical explosives and nuclear explosives.

As illustrated in Fig. 1, there are analogies between the different phenomena in chemical and nuclear explosions at early times, but the mechanical effects at later times are identical --except as may be determined by differences of scale. The nuclear explosive is analogous to the primary chemical explosive or initiator; and the vaporization of the rock in the nuclear explosion is analogous to the detonation of the secondary or high

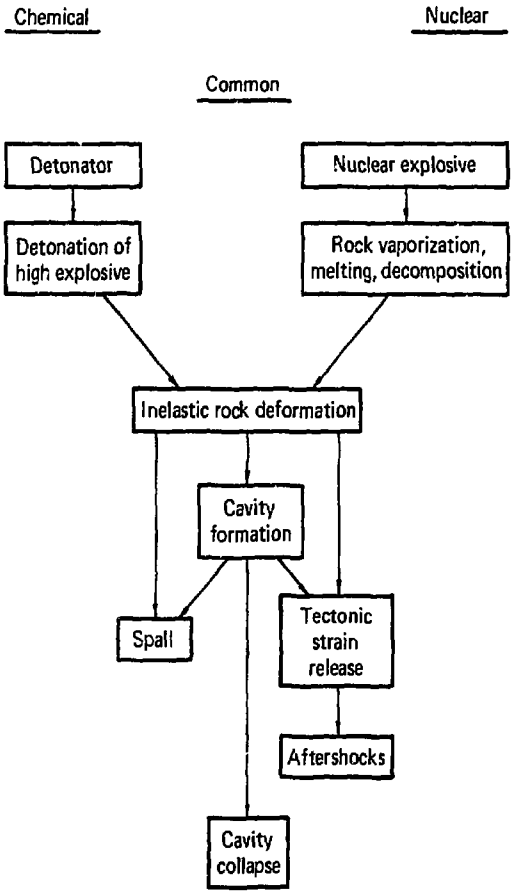

FIG. 1. Processes in underground chemical and nuclear explosions.

explosive. The subsequent inelastic rock deformation and seismic wave generation are fundamentally identical in both types of explosions.

There are generally large differences of scale between chemical and nuclear explosions. There have been only a few chemical explosions with yields of more than a kiloton [1 kiloton (kt) = 4.18 terajoules (TJ)], but there have been several nuclear explosions with yields of a megaton or more (Springer and Kinnaman 1971, 1975). The problems of seismic detection, identification, and yield estimation are comparatively simple for megaton-class explosions, but are challenging and often difficult for subkiloton

to kiloton explosions. There are no known seismic techniques for remote discrimination between chemical and nuclear explosions of comparable yield.

2.1 Initial Conditions in Chemical and Nuclear Explosions

The function of the primary chemical explosive or initiator is to generate the conditions for detonation of the secondary explosive. Primary explosives like mercury fulminate and lead azide detonate when heated. If such a detonation occurs in sufficiently close proximity to a secondary explosive like TNT or RDX, the resulting shock compression can initiate detonation of the secondary explosive. The conditions in the detonation wave in RDX are pressures of several hundred thousand standard atmospheres and temperatures of 5000 to 6000°K (Johansson and Persson 1970, Chs. 1,2).

When the reactions in a nuclear explosive are completed, the explosive materials have been transformed into an ionized gas at a pressure of millions of atmospheres and a temperature of millions of degrees Kelvin. The 1.7-kt Rainier explosion was in an underground chamber having a volume of 7 m^3 and containing a mass of material of about 1 tonne (t). It was estimated that a few microseconds after detonation, the pressure in that chamber was about 7 million atm and the temperature was about 10^6 °K (Johnson, Higgins, and Violet 1959).

2.2 Nuclear Explosions: Rock Vaporization

The extremely high pressures produced by the detonation of a buried nuclear explosive generate a strong shock wave that propagates outward into the surrounding rock. Shock compression is an irreversible thermodynamic process that deposits thermal energy in the rock. For very strong shock waves, the energy deposition is sufficient to vaporize the rock. For a nonporous silicate rock like granite, the shock pressure required for vaporization is estimated to be about 2 million atm; for porous silicate rocks like tuff or alluvium, the required shock pressure is estimated to be about one-third to one-half that value (Butkovich 1967).

A shock wave is attenuated as it propagates outward from the center of an explosion, and the thermal energy deposition decreases accordingly. There is a range in which the energy deposition is insufficient for vaporization but sufficient to melt the rock. Some rocks, such as dolomite, do not melt but decompose and sublime instead.

The vaporized rock, which is initially at a pressure of a million or more atmospheres, expands and does mechanical work on the surrounding rock until an equilibrium is established between

the cavity pressure and the resisting stresses in the surrounding rock. This expansion process is described further in Section 2.7.

2.3 Chemical Explosions: Explosive Detonation

The detonation of a buried charge of secondary explosive is analogous in one sense to the vaporization of rock in a nuclear explosion: the result of both processes is a gas that expands and does mechanical work on the surrounding rock. There are also differences between the two processes. The rock vapor is initially at much higher pressures and temperatures than the detonation products of the chemical explosive. Rock vaporization absorbs explosive energy, but chemical explosive detonation releases energy. The energy release in underground chemical explosions is not sufficiently intense to vaporize any surrounding rock. But special chemical explosive assemblies can be designed to vaporize metals. See Zel'dovich and Raizer [1967, Ch. XI (4) 21-22] and Ahrens and Urtiew (1971).

2.4 Inelastic Rock Deformation

In underground explosions, a strong shock wave is propagated outward into solid rock from the cavity containing either explosive detonation products (in the case of a chemical explosion) or rock vapor and melt or decomposition products (in the case of a nuclear explosion). In either case, the initial shock wave pressure is generally on the order of several hundred thousand atmospheres (except, for example, when the explosive is emplaced in a large cavity for seismic-decoupling purposes; this special condition is discussed in Section 6.1). The shock pressure is attenuated as the shock wave propagates outward; partly because of the geometry of a diverging wave, but also because of the irreversible thermodynamic processes in the shock wave. At very high pressures, solid-solid phase changes may occur because of thermodynamic nonequilibrium during shock loading and unloading. An example is the transition of quartz into coesite or stishovite. At sufficiently high pressures, the shear stresses are negligible and the rock deforms as if it were a fluid. At somewhat lower pressures, the shear stresses are significant and the rock is plastically deformed. At still lower pressures, the rock may fracture in shear or tension. Porous rocks will be crushed and permanently compacted at sufficiently high pressures. If the pores are partially- or fully-saturated with a liquid (usually water), the crushing and compaction are reduced and other mechanical properties are modified. Finally, there is some ill-defined boundary called the "elastic radius" beyond which nonlinear inelastic deformation does not occur, but linear anelastic processes continue to attenuate the "elastic" waves from the explosion. Inelastic deformation and the "elastic radius" are discussed further in Section 3.4.

2.5 Tectonic Strain Release

Early in the history of underground nuclear explosions, seismological and geological evidence began to accumulate that some underground nuclear explosions released preexisting tectonic strain. Most of the evidence was in the form of Love- and Rayleigh-wave radiation patterns. Two principal hypotheses have been advanced to explain the observed tectonic strain releases. One is release of the preexisting tectonic strain around the inelastic zone surrounding the explosion (the tectonic strain field responds to the creation of a weak fractured zone around the explosion). The other hypothesis is triggering of a dislocation along a nearby fault plane. The first hypothesis appears to be satisfactory in many cases, but the triggering hypothesis is favored in cases with relatively large amounts of tectonic strain release. Tectonic strain release is discussed further in Section 4.1.

2.6 Spall

The stress waves that propagate upward from an underground explosion are reflected at the free surface because of the impedance mismatch between the surface layer and the atmosphere. Other reflections may occur below the surface if the geological structure is layered, with different densities and elastic moduli in adjacent layers.

The principal outgoing wave from an explosion is a compressional wave; it is reflected from the free surface as a rarefaction wave. Rocks generally have low tensile strength; consequently, the downgoing reflected wave may cause the rock to fail in tension at some point below the surface. This failure occurs while the mass of rock above the region of tensile failure has a net upward momentum. The spalled layer enters a ballistic trajectory that eventually ends in "slapdown" when the gap opened by the spalling process is closed. Some evidence suggests that spall "slapdown" is a significant seismic wave source under some conditions. Spall is discussed further in Section 4.2.

An interesting related phenomenon, observed in connection with several nuclear tests in the Yucca Flat testing area of the Nevada Test Site, is the occurrence of multiple reflections of compressional and rarefaction waves between the free surface and the underlying rocks of Paleozoic age beneath Yucca Flat. There is a considerable impedance mismatch between these Paleozoic rocks and the overlaying aluminum and tuff. Displacement time histories from several velocity gauges from one nuclear test are shown in Fig. 2, and the Fourier spectrum of the signal from one of these gauges is given in Fig. 3. It was found that the wave period is

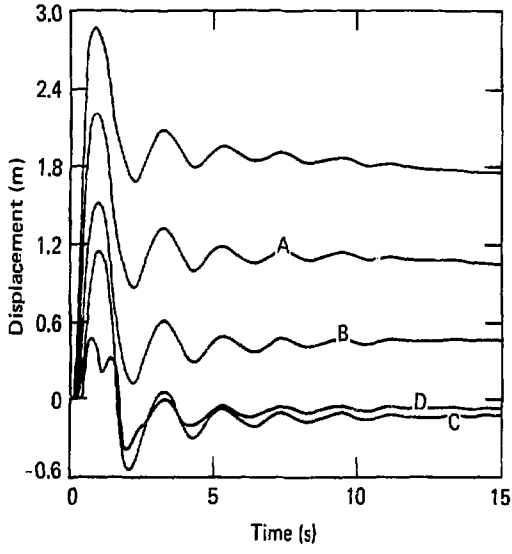

FIG. 2. Vertical compressional-wave resonance in Yucca Flat at the Nevada Test Site. Integrated velocity-gauge signals from Starwort: (top) gauge 22 UV, (A) gauge 23 UV, (B) gauge 24 UV, (C) gauge 25 UV, and (D) gauge 51 UV (from Wheeler, Preston, and Frerking, 1976).

equal to four compressional wave transit times between the free surface and the Paleozoic rock surface, and this resonance period is independent of explosion yield and depth. The velocity gauge data were examined for a total of eight tests; this resonance was found in seven of the eight cases (Wheeler, Preston, and Frerking 1976).

This resonance phenomenon may be related to Rayleigh wave generation by explosions. In a theoretical study, Hudson and Douglas (1975) noted that when a sharp impedance contrast exists in a plane-layered model of the crust, the Rayleigh wave group velocity minimum in the fundamental mode occurs close to a period equal to four times the travel time of P-waves from the surface to the interface.

2.7 Cavity Formation and Residual Stresses

The cavity gases, either rock vaporized in a nuclear explosion or detonation products of a chemical explosion, are initially at a pressure of several hundred thousand atmospheres or more. This pressure is applied to the surrounding rock in the

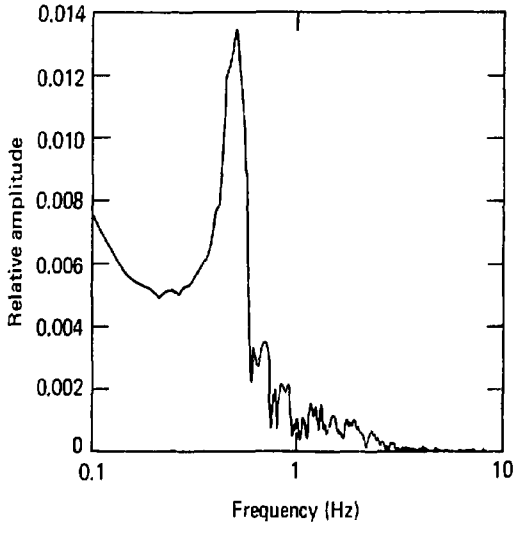

FIG. 3. Vertical compressional-wave resonance in Yucca Flat at the Nevada Test Site. Fourier spectrum of the signal from velocity gauge 23 UV (Fig. 2) in Starwort: time interval is 4 to 30 s of signal record (from Wheeler, Preston, and Frerking, 1976).

case of a "tamped" explosion (the special case of an explosion in a large preexisting cavity is discussed in Section 6.1). The effects of this pressure are not only the generation of a shock wave that inelastically deforms the rock (discussed in Section 2.4), but also the outward displacement of the surrounding rock as the cavity expands. The outward propagation of the principal inelastic stress wave and the cavity growth are intimately related at early times when rock is being vaporized. When rock vaporization no longer occurs, the stress wave "breaks away" from the cavity boundary, and cavity expansion becomes independent of the principal outgoing stress wave--until this wave returns as a rarefaction wave reflected from the free surface. Except for perturbations by the surface reflection, the later phases of cavity dynamics are functions of the thermodynamic properties of the cavity gases, the mechanical properties of the surrounding rock, and the overburden pressure. The final dynamic cavity pressure of a contained explosion may range from one-third to twice the initial overburden pressure, depending upon the mechanical properties of the surrounding rock. The creation of this cavity results in a significant change in the stress pattern in the surrounding rock. These stress changes are probably related

to the aftershocks that are sometimes observed following an underground explosion.

The phenomena of rock vaporization, inelastic rock deformation, and cavity expansion are schematically illustrated in Fig. 4.

2.8 Cavity Collapse and Aftershocks

After the explosion, any coincident tectonic strain release, and spall have occurred, two explosion-related phenomena can generate seismic signals at later times: cavity collapse and aftershocks.

In general, the cavities produced by contained explosions are not stable. The only known exceptions are cavities in salt formations; e.g., those produced by the 3-kt Gnome (Rawson 1963) and 5.3-kt Salmon (Rawson, Taylor, and Springer 1967) explosions in the U.S., and by 1.1- and 25-kt explosions in the USSR (Kedrovskii 1970).

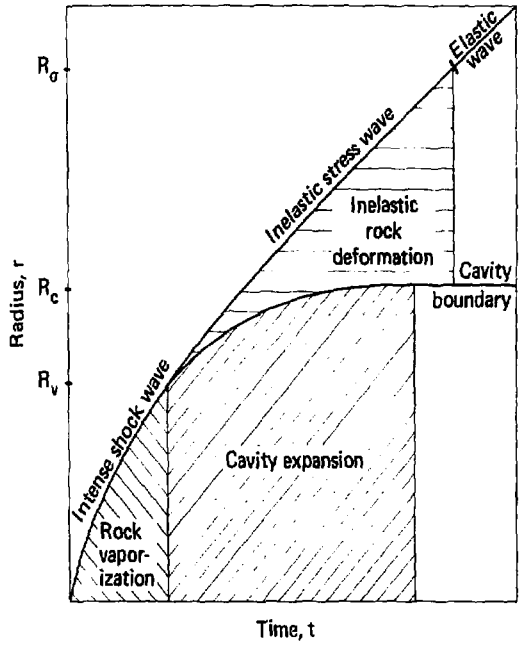

FIG. 4. Radius-vs-time relation for an underground nuclear explosion with regard to rock vaporization, cavity expansion, and inelastic rock deformation (from Rodean 1971a).

Cavity collapse forms a "chimney" which may or may not extend to the surface, forming a subsidence crater (Boardman, Rabb, and McArthur 1964). Springer and Kinnaman (1971, 1975) list surface collapse intervals that have been observed following US nuclear explosions; the intervals range from minutes to hours--and even years in a few exceptional cases. Smith (1963) compared P, SV, and Rayleigh waves from explosions and subsequent cavity collapses at the Nevada Test Site. He noted that the amplitudes of these phases from collapses are significantly smaller than from the corresponding explosions. He also noted that the phases of Rayleigh waves from collapses are reversed relative to those from the corresponding explosions. These observations have been confirmed by others, including McEvilly and Peppin (1972) who also found that the Rayleigh to P_n amplitude relations for collapses are similar to those for earthquakes and explosion aftershocks, and different from those for explosions.

It was noted in the preceding section that the formation of a cavity by an underground explosion changes the stress distribution in the surrounding rock. Brune and Pomeroy (1963) found that small earthquakes were triggered near the site of the Hardhat explosion. Boucher, Ryall, and Jones (1969) reported the results of a preliminary study which showed that increases in seismic activity followed underground nuclear explosions in Nevada with seismic magnitudes of 5 and greater. Hamilton et al. (1972) presented the results of an extensive investigation of aftershocks following five high-yield underground nuclear explosions in the Pahute Mesa area at the Nevada Test Site. Four of the five explosions initiated earthquake or aftershock sequences lasting from 10 to 70 days. The number of magnitude 2.0 or larger aftershocks in these sequences ranged from 24 to 2,012; all magnitudes were less than 5.0. Ninety-four percent of the aftershocks with well-determined depths occurred at depths less than 5 km, and 95 percent of the located aftershocks were within 14 km of ground zero of the preceding explosion. Engdahl (1972) presented the different results of a similar study following Milrow and Cannikin on Amchitka Island. Each explosion was followed by hundreds of discrete events which were apparently related to cavity collapse. This activity intensified and then terminated within minutes of surface subsidence at the explosion sites (Milrow, 37 hours; Cannikin, 38 hours). The aftershock sequences following these explosions were less extensive and shorter than those observed in Nevada. Israelson, Slunga, and Dahlman (1974) reported an aftershock sequence within a 4-hour period following a large underground nuclear explosion at the southern end of Novaya Zemlya. McEvilly and Peppin (1972) found that the Rayleigh to P_n amplitude relations for aftershocks are different from those for explosions at the Nevada Test Site.

2.9 Thermal Effects

It was noted in preceding sections that shock (inelastic stress) waves involve irreversible thermodynamic processes that deposit thermal energy and produce irreversible deformation in the rock. Analysis of postshot rock temperatures for eight nuclear explosions at the Nevada Test Site indicates that 90 to 95 percent of the total energy released is deposited as residual thermal energy if the explosion is completely contained (Heckman 1964). More detailed thermal analysis of the Salmon explosion indicates that about 90 percent of the total energy released was deposited within 50 m of the explosion (Edwards and Holzman 1968). This percentage does not include the energy dissipated in crushing and fracturing the salt out to 90 m from the edge of the 17-m-radius Salmon cavity (Rawson, Taylor, and Springer 1967).

3. SPHERICAL EXPLOSIONS: THEORY AND MEASUREMENTS

A contained underground nuclear explosion is, generally, approximately spherical. This sphericity is convenient because it permits one to model an explosion in only two variables: time and a radial spatial coordinate. In this section, it is assumed that the geometry of explosions is spherical; nonspherical geometry is considered in the following section. In the remainder of this lecture, all explosions are understood to be nuclear, except when explicitly identified as chemical.

3.1 Simple Theoretical Models

A number of simple theoretical models have been developed to represent explosions; a selected few are described in the following paragraphs. These models demonstrate some of the physical principles involved in explosions, and certain mathematical solutions define upper or lower limits for some phenomena.

The simplest physical system used to model seismic wave radiation from explosions and earthquakes is a spherical cavity in a homogeneous, isotropic, infinite elastic solid. Solutions for the output (compressional elastic wave motion) as functions of time and the radial spatial coordinate may be obtained as functions of the input (cavity pressure variation with time) and the following parameters: cavity radius, medium density, and the Lamé constants (λ and μ) that define the elastic properties of the solid. Jeffreys (1931) used the assumption that $\lambda = \mu$ in obtaining the first solution of this problem; Kawasumi and Yosiyama (1935) were the first to obtain a general solution in terms of λ and μ. We will use this model in several subsequent parts of this lecture. For the present, we will use the result that, in our assumed

elastic solid, the peak particle velocity in a spherical wave in the far field varies as

$$u \propto r^{-1}, \tag{1}$$

where u is the peak particle velocity and r is the radial coordinate in space. This relation is consistent with zero inelastic energy dissipation because the kinetic energy in the wave is proportional to $u^2/2$, the surface area of a sphere with radius r is $4\pi r^2$, u varies inversely with r [Eq. (1)], and the product $(u^2/2)(4\pi r^2)$ is proportional to the constant 2π.

An ideal elastic medium is a useful mathematical fiction; all real materials are inelastic to some degree, even at very low stress levels. This "almost elastic" behavior of solid materials is often called "anelastic" or "viscoelastic." The mathematical solutions for wave propagation in anelastic or viscoelastic solids are more complex than in the elastic case. Viecelli (1973a) obtained a similarity solution for a spherical compressional wave in a viscoelastic solid described by the Voigt model. His analytic result is the asymptotic solution for the wave generated by a spherical cavity expanding at constant velocity. He found that

$$u \propto r^{-3/2} \tag{2}$$

in the far field. In this case, the kinetic energy in the wave is dissipated by viscous effects as indicated by the product $(u^2/2)(4\pi r^2)$ being proportional to $2\pi r^{-1}$.

In work done during World War II, but published later, Sedov (1959) in the USSR, Taylor (1950a) in the United Kingdom, and von Neumann (1963) in the US independently obtained similarity solutions for an intense point explosion, a simple model for a nuclear explosion. Taylor (1950b) successfully applied his solution to the analysis of the first nuclear explosion. This was Trinity, an atmospheric explosion in New Mexico in 1943. The point source solution is also a good approximation to the initial stage of an underground nuclear explosion because, at early times, the rock vapor is a highly ionized gas. The properties of such a high temperature, high pressure gas are independent of initial chemical composition and crystalline structure. In the point-source solution,

$$u \propto r^{-3/2}. \tag{3}$$

Surprisingly, this result is identical to the viscoelastic solution given by Eq. (2). Perhaps this is because both are similarity solutions.

Zel'dovich and Raizer [1967, Ch. XII (4) 21] presented a solution for a strong explosion in an infinite porous medium. They assumed that the porous medium is compressed to the density of the continuous medium, and that the continuous medium is incompressible. In other words, they assumed that the shock is strong with respect to the strength of the porous material, but weak with respect to the compressibility of the continuous material. They found that

$$u \propto r^{-3n/2}, \tag{4}$$

where n is bounded by the limits $n > 1$ (approaching zero medium porosity) and $n < 2$ (approaching 100 percent porosity).

The radial variations of the peak radial stress (above equilibrium) for the three cases corresponding to Eqs. (1), (3), and (4) are also of interest. For an elastic wave, corresponding to Eq. (1),

$$\Delta\sigma_r \propto r^{-1}. \tag{5}$$

For a strong shock in a continuous medium, corresponding to Eq. (3),

$$\Delta\sigma_r \propto r^{-3}. \tag{6}$$

For a strong shock in a porous medium, corresponding to Eq. (4),

$$\Delta\sigma_r \propto r^{-3n}, \tag{7}$$

where $1 < n < 2$ as in Eq. (4).

3.2 Stress Wave Measurements in Geological Media

Peak-radial-stress measurements in the vicinity of a number of underground nuclear explosions are presented in Fig. 5. These explosions in alluvium, dolomite, granite, salt, and tuff had yields on the order of 10 kt. The data, replotted from a study by Holzer (1966), are scaled to a yield of 1 kt (scaling is discussed in Section 6.2). The shock pressures for vaporization are approximately 100 GPa (1 Mbar) and the radii of vaporization are about 2 $m/kt^{1/3}$ for these materials (Butkovich 1967). Therefore, the reference curve for the strong-shock solution is not necessarily arbitrarily drawn through the point 100 GPa (1 Mbar), 2 $m/kt^{1/3}$. As noted in Rodean (1971a), the following conclusions can be made from Fig. 5:

- The data for nuclear explosions in all five materials tend toward a common strong-shock solution at peak radial stresses greater than 10 GPa (100 kbar) and scaled radii of a few meters.

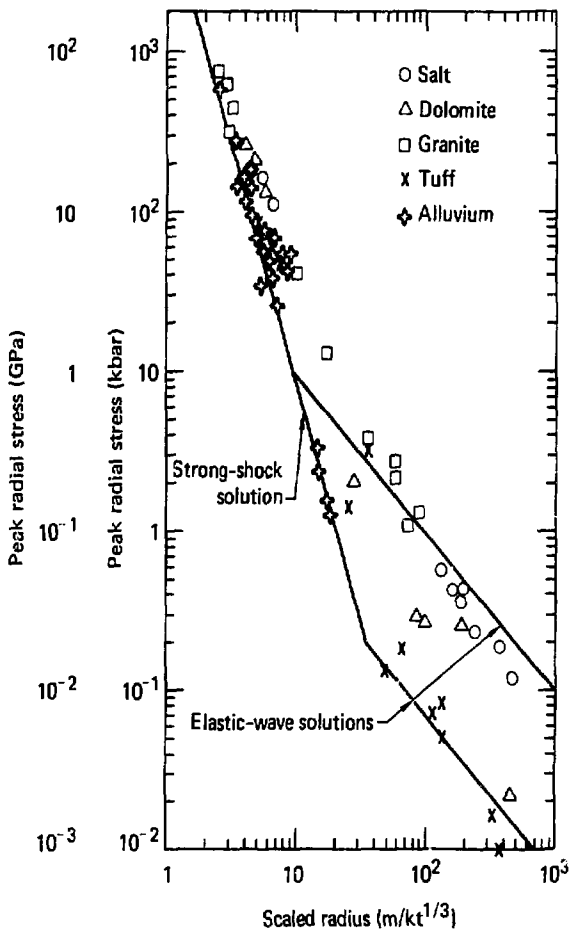

FIG. 5. Measurements and two theoretical solutions for peak (above equilibrium) radial stress produced by underground nuclear explosions (from Rodean 1971a).

- The data for the porous materials, alluvium and tuff, tend to follow the strong-shock solution down to peak radial stresses of about 0.1 GPa (1 kbar).

- The data for granite and salt are so similar that a common curve could be fitted to the points for both materials.

- The data for dolomite are similar to those for granite and salt at scaled radii of a few meters and peak radial stresses above 10 GPa (100 kbar), but the peak radial stresses are intermediate between those in granite and salt and those in tuff at scaled radii of tens and hundreds of meters.

- At scaled radii of hundreds of meters, the data for dolomite, granite, salt, and tuff tend toward (but do not reach) the elastic wave solution.

There are three categories of stress levels surrounding an underground nuclear explosion which must be considered in studying the effects of rock properties on seismic coupling. The first is the very high stress or hydrodynamic region in which the effects of material properties, such as strength, are negligible. This region is illustrated in Fig. 5 at stresses approaching 100 GPa (1 Mbar) and scaled radii of a few meters. The second is the moderate-stress region where material strength has a significant effect and the rock behavior is definitely inelastic. This region corresponds approximately to stresses of 10^{-1} to 10^{1} GPa (1 to 100 kbar) and scaled radii from ten to a few tens of meters in Fig. 5. The third is the low-stress region in which the material response tends toward elastic behavior. In Fig. 5, this region corresponds approximately to stresses less than 10^{-1} GPa (1 kbar) and scaled radii on the order of 100 m and greater. The relative importance of these regions in seismic coupling is a strong function of material properties; however, the lower-stress regions tend to dominate coupling because more of the rock surrounding an explosion is subjected to the lower stresses (the volumetric contribution is proportional to r^3).

In 1970, Larson (1977a) began a comprehensive experimental investigation of the effects of rock properties on seismic coupling efficiency, with emphasis on the moderate- and low-stress regions. He conducted a series of small-scale high-explosive experiments in the 15 geological materials listed in Table 1. Westerly granite and Nugget sandstone were selected to represent high-strength, low-porosity rocks, and Blair dolomite and polycrystalline salt were chosen to represent moderate- to low-strength, low-porosity rocks. Dry Mt. Helen tuff and Indiana limestone were chosen to represent rocks with large values of dry porosity. Water-saturated samples of the latter two rocks, saturated Tunnel tuff, and water were selected to demonstrate the effects of water saturation. Ice and two frozen soils, Ottawa banding sand and West Lebanon glacial till, were included to represent permafrost and to provide information on the effects associated with the melting-ice phase transition. The data on the Kemmerer coal were available and included for the sake of completeness.

TABLE 1. Properties of the fifteen geologic materials selected for study by Larson (1977a).

Geologic material	Bulk density (Mg/m^3)	Dry porosity (%)	Longitudinal sound speed[a] (km/s)
Westerly granite	2.65	1	4.80
Nugget sandstone	2.55	4	3.45
Blair dolomite	2.84	1	5.00
Polycrystalline NaCl	2.13	1.6	4.10
Mt. Helen tuff (dry)	1.46	40	2.75
Mt. Helen tuff (saturated)	1.86	0	2.60
Indiana limestone (dry)	2.28	16	4.20
Indiana limestone (saturated)	2.37	8	4.35
Tunnel tuff (saturated)	1.73	14	-
Ice	0.92	0	3.35
Frozen Ottawa banding sand (ice saturated)	2.03	0	4.40
Frozen West Lebanon glacial till (ice saturated)	2.08	5.5(?)	3.45
Frozen West Lebanon glacial till (50% ice saturated)	1.96	19	2.50
Water	1.00	0	1.45
Kemmerer coal	1.30	0	2.25

[a]Or compressional wave velocity.

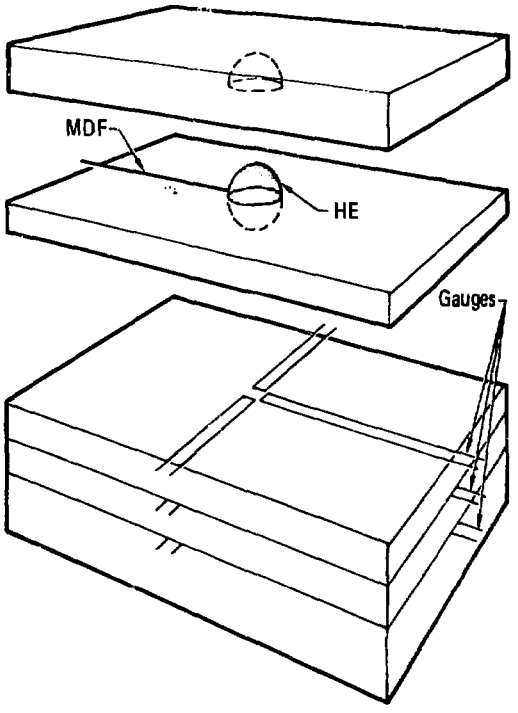

FIG. 6. Schematic drawing of Larson's (1977a) high-explosive (HE) experimental assemblies for dynamic stress-wave measurements in geological materials. The LX04 HE is initiated with a mild detonating fuse (MDF) attached to a detonator within the sphere of HE. The entire assembly is placed in the center of a large electromagnet when the experiment is conducted.

Larson's experimental assemblies are schematically illustrated in Fig. 6. The assemblies formed a cube about 0.35 m on a side. The high-explosive spherical charges had radii of either 1.9×10^{-2} m or 9.5×10^{-3} m. Gauges, placed radially from the spherical explosive charges as shown in Fig. 6, recorded particle velocity and radial-stress time histories.

Larson compared seismic coupling efficiency using peak particle velocity and peak radial stress attenuation as functions of scaled radius (in this case, the ratio of the radial distance to the gauge to the radius of the explosive charge). The experimental results for a strong, low-porosity rock (Westerly granite)

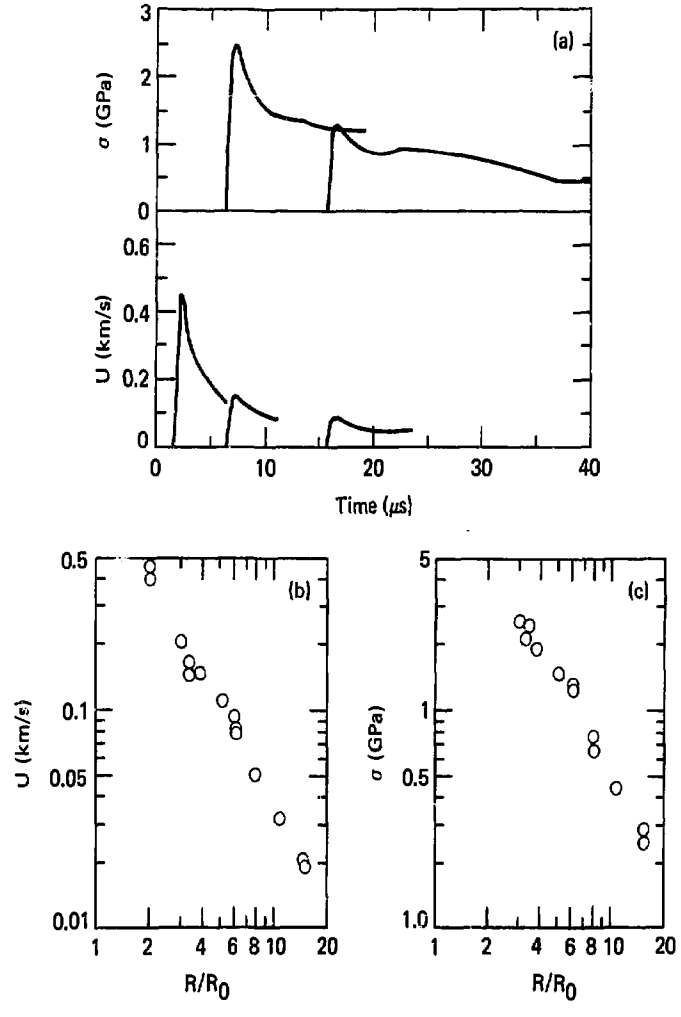

FIG. 7. Experimental results for Westerly granite: (a) particle-velocity and stress vs time, (b) peak particle-velocity vs reduced radius, and (c) peak stress vs reduced radius (from Larson 1977a).

and for a weak, high-porosity rock (dry and saturated Mt. Helen tuff) are presented in Figs. 7, 8, and 9, respectively. Note the steep stress-wave fronts in the granite [Fig. 7(a)] and the dispersive stress waves in the tuff [Figs. 8(a) and 9(a)]. Also note that water saturation reduces the stress-wave attenuation and

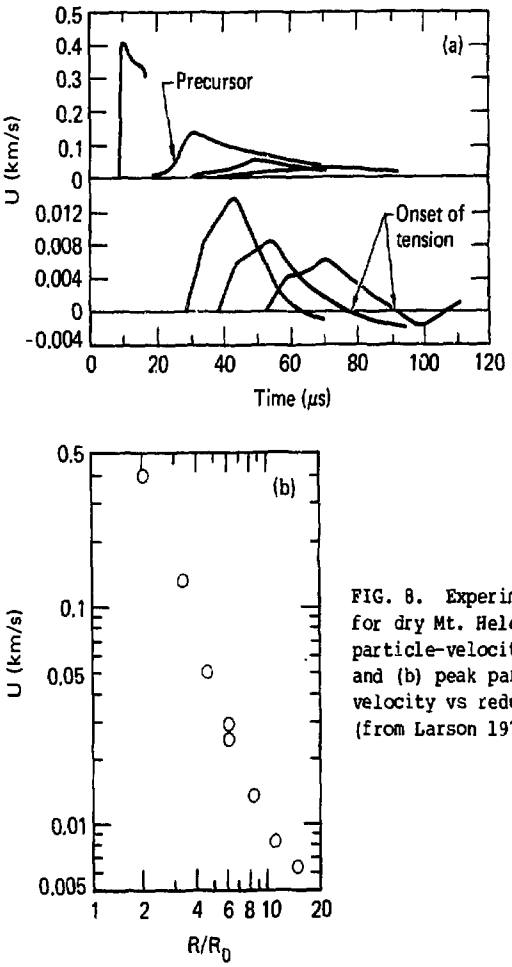

FIG. 8. Experimental results for dry Mt. Helen tuff: (a) particle-velocity vs time, and (b) peak particle-velocity vs reduced radius (from Larson 1977a).

dispersion in tuff [Figs. 8(b) and 8(a) for dry vs Figs. 9(b) and 9(a) for saturated tuff]. The data for H_2O in two natural states are compared in Figs. 10 (water) and 11 (polycrystalline ice). Note that the stress waves are more dispersive and that the stress-wave attenuation is greater in ice than in water. The extremes of stress-wave attenuation, from the lowest to the highest, for these 15 geological materials are summarized in Figs. 12 and 13. The lowest attenuation was observed in water, the lowest attenuation observed in rock was in granite, and the highest attenuation observed in rock was in dry Mt. Helen tuff; these data are presented in Fig. 12. The attenuation for water and the frozen materials is presented in Fig. 13; the attenuation in 50% saturated

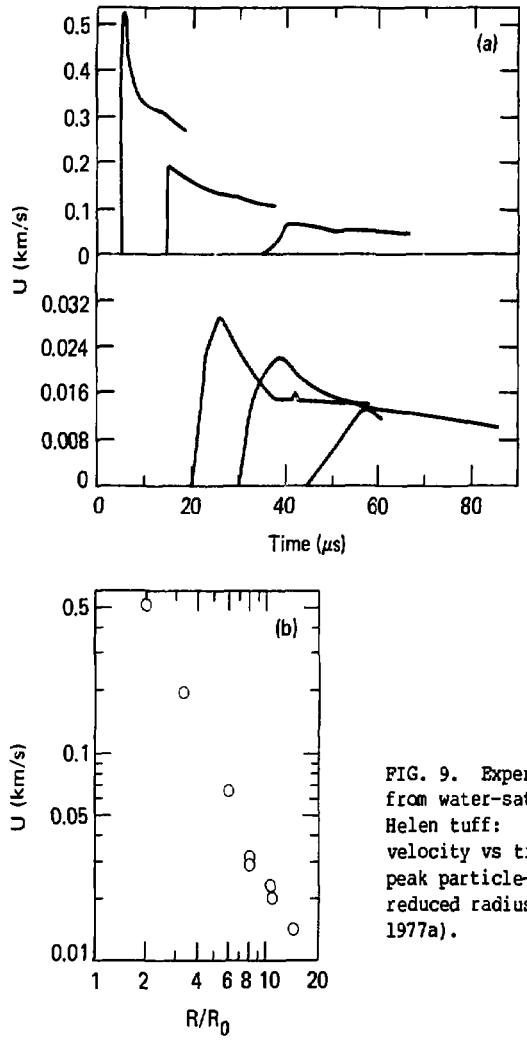

FIG. 9. Experimental results from water-saturated Mt. Helen tuff: (a) particle-velocity vs time, and (b) peak particle-velocity vs reduced radius (from Larson 1977a).

West Lebanon glacial till was the highest observed in all the materials tested.

Larson found that the peak-particle velocity attenuation in the 15 geological materials could be approximated by the relation $u \propto r^{-n}$ where u is peak-particle velocity, r is scaled radius, and n is an empirical constant. His attenuation exponent data are summarized in Table 2 and are compared with attenuation exponents

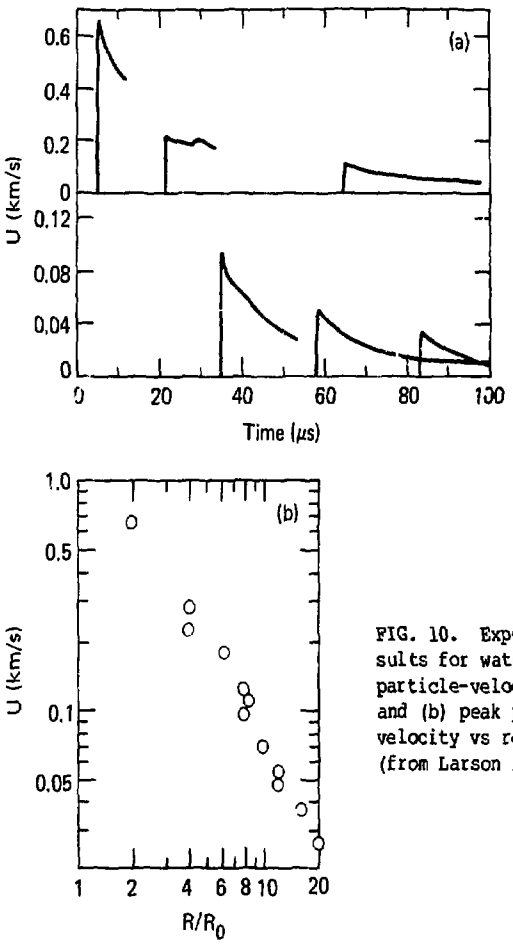

FIG. 10. Experimental results for water: (a) particle-velocity vs time, and (b) peak particle-velocity vs reduced radius (from Larson 1977a).

from the theoretical models represented by Eqs. (1)-(4). Note that none of the materials exhibited ideal elastic behavior (n = 1), that water and the low-porosity rocks approximated visco-elastic or strong-shock behavior (n = 1.5), and that the behavior of the porous rocks is bracketed by the strong-shock response of a porous solid (n = 1.5 to 3). Larson's conclusions include the following:

- The large difference between the peak-particle velocity attenuation relation for water, $r^{-1.4}$, and that for an ideal elastic solid in the far field, r^{-1}, is attributed to viscosity and finite strain. In consolidated rocks, the observed limiting

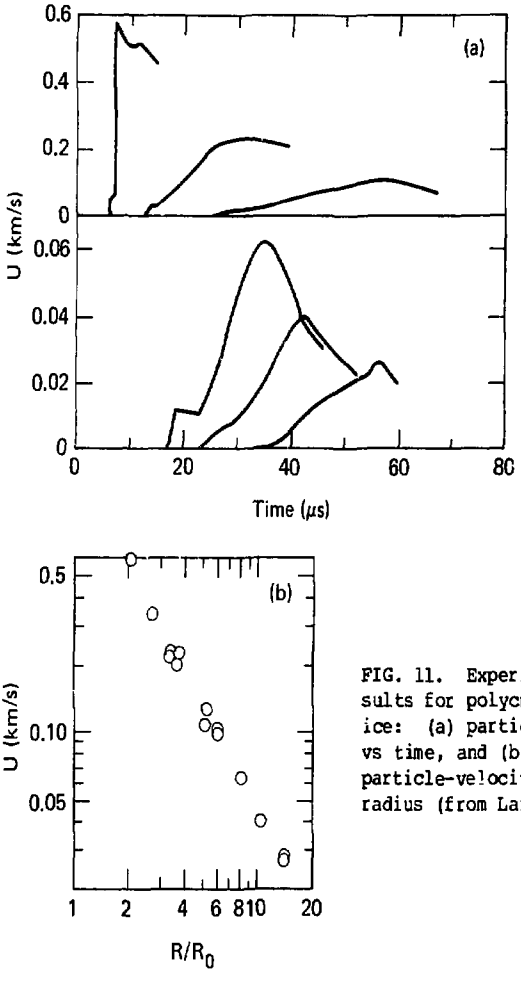

FIG. 11. Experimental results for polycrystalline ice: (a) particle-velocity vs time, and (b) peak particle-velocity vs reduced radius (from Larson 1977a).

attenuation relation, $r^{-1.5}$, is attributed to viscosity and finite strain, as well as to the presence of microcracks and other grain-boundary effects. These attenuation rates appear to be limiting values for real materials.

• The large difference in coupling between water, $r^{-1.4}$, and water-saturated Mt. Helen tuff, $r^{-1.9}$, suggests that two-component interactions lead to both dispersion and dissipation as the wave propagates through saturated rock. The smaller attenuation observed in water-saturated coal, $r^{-1.6}$, is attributed to the absence of two-component interactions. This absence is the

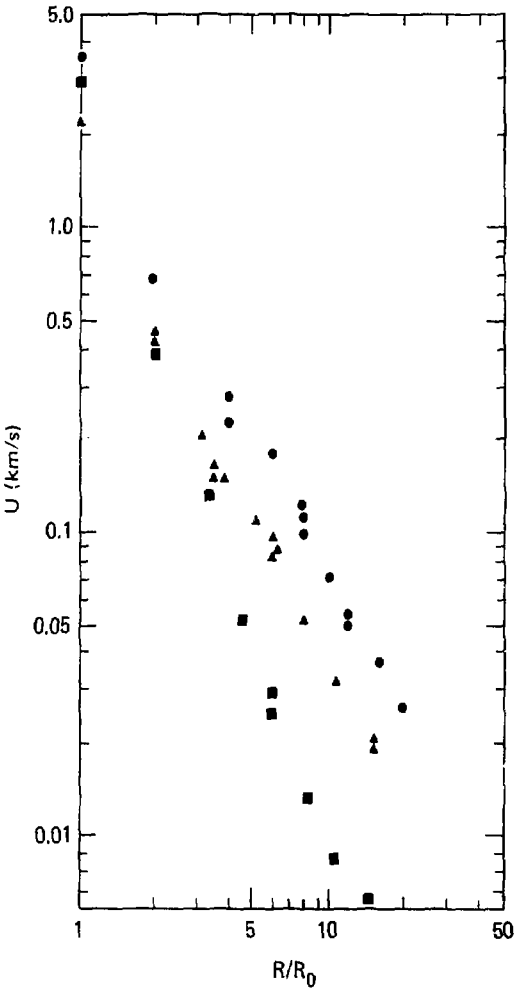

FIG. 12. A comparison of peak particle-velocity attenuation for water (●), Westerly granite (▲), and dry Mt. Helen tuff (■) (from Larson 1977a).

result of chemical bonding of the water into the coal matrix. The attenuation that does occur in coal is caused by grain-boundary effects that are associated with the highly fractured structure.

● The difference in coupling between water, $r^{-1.4}$, and ice, $r^{-1.5}$, is attributed to the ice-I melting transition. Introduction of soil into the ice matrix causes a significant

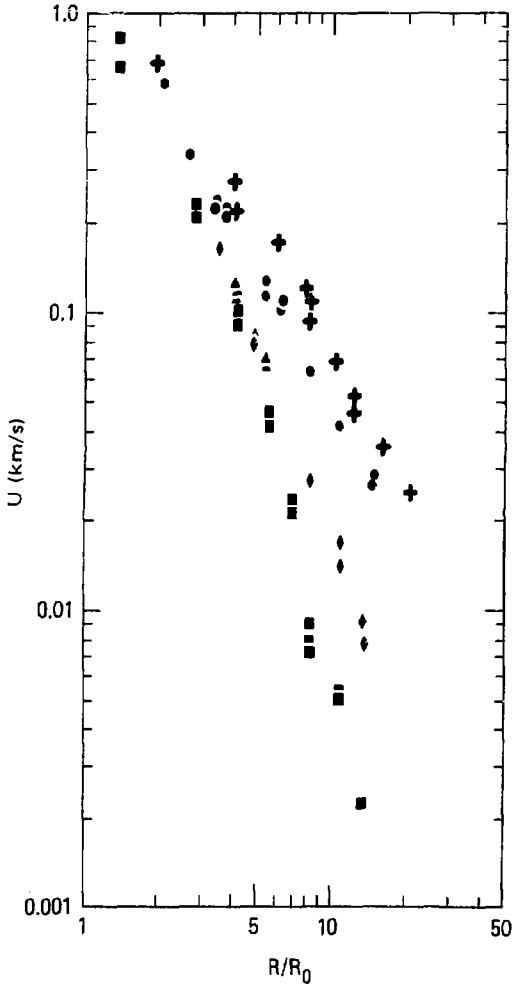

FIG. 13. A comparison of peak particle-velocity attenuation for water (+) and frozen materials: ice (●), Ottawa bonding sand (▲), 50% ice-saturated West Lebanon glacial till (▬), and 100% ice-saturated West Lebanon glacial till (◆) (from Larson, 1977a).

increase in attenuation rates to $r^{-2.0}$. This increased dissipation is thought to be associated with hysteresis in the transition that results from the presence of the soil. The coupling in 50% ice-saturated soil, $r^{-2.7}$, is probably the

TABLE 2. Exponents for radial attenuation of peak particle velocity observed in small-scale high-explosive experiments in 15 geological materials (Larson 1977a). Theoretical attenuation exponents are presented for reference from Eqs. (1)-(4).

	Exponent n for radial attenuation ($u \propto r^{-n}$)		
	Low stresses	Overall average	High stresses
[Far-field elastic wave, Eq. (1)]		(1.0)	
Water		1.4	
[Viscoelastic wave, Eq. (2); strong shock, Eq. (3)]		(1.5)	
Ice		1.5	
Westerly granite		1.5	
Nugget sandstone		1.5	
Blair dolomite		1.6	
Kemmerer coal		1.6	
Polycrystalline NaCl		1.6 to 1.8	
Indiana limestone (saturated)	1.4		2.2
Indiana limestone (dry)	1.6		2.4
Mt. Helen tuff (saturated)		1.9	
Mt. Helen tuff (dry)	1.5		2.5
Tunnel tuff (saturated)		2.1	
Both frozen soils (saturated)		2.0	
Frozen West Lebanon glacial till (50% saturated)		2.7	
[Strong shock in a weak porous solid, Eq. (4)]		(1.5 to 3.0)	

result of the yielding of the weak ice matrix which allows pore collapse at very low stresses.

- For rocks and soils with significant dry porosity, the peak-particle velocity attenuation relation ranges from $r^{-2.5}$ to $r^{-2.7}$. For these materials, dissipation of energy in crushing pores dominates all other inelastic mechanisms and continues until a stress is reached that corresponds to matrix strength.

- Therefore, the order of importance for material properties in determining relative coupling is (1) porosity, (2) strength, (3) multiple-component interactions, and, in frozen materials, (4) phase transformation.

One may ask, "What is the quantitative relation between the data from nuclear explosions and the data from small-scale experiments with high explosives?" Larson successfully scaled his small scale, high explosive, peak particle-velocity data for salt (NaCl) to the data for the 5.3-kt Salmon explosion in salt (Rogers 1966). Trulio (independently and simultaneously) found that the data from the higher-yield Cowboy experiments with tamped high-explosives (Murphey 1961) could be scaled with equal success to the Salmon data (Larson 1977b; Trulio 1977).

A result of their subsequent joint work is presented in Fig. 14: the data from the latter three sources, scaled over eight orders of magnitude of explosive energy release (see Section 6.2 for a discussion of scaling), form a common peak-particle velocity vs scaled radius relation over corresponding large ranges of velocity and radius. The combined data are approximated by the relation $u \propto r^{-1.7}$, which is consistent with the exponent values of -1.6 to -1.8 given in Table 2 for Larson's data alone. [Attempts to scale data from small-scale high-explosive experiments and nuclear-explosion data in other materials have not been successful (Larson 1977b). These failures are attributed to large-scale inhomogeneities, such as block motion, in the nuclear explosions, or to differences in material properties for the two sets of explosions.]

With respect to the above, particle-velocity data that fit a relation $u \propto r^{-n}$, with $1 < n < 2$, *can* represent elastic behavior. This is because $u \propto r^{-1}$ in the far field [Eq. (1)], but nearer the source, the term $u \propto r^{-2}$ also contributes to the particle velocity in spherical elastic waves [Eq. (30)]. The transition between the near and far fields for particle velocity, at which the contributions of the near and far field terms [Eq. (30)] are equal in amplitude, is defined by the relation $r\omega = \alpha$ (Meyer 1964) where r is the radial coordinate, ω is the angular frequency, and α is the compressional wave velocity. The far field effects are dominant only if $r\omega >> \alpha$.

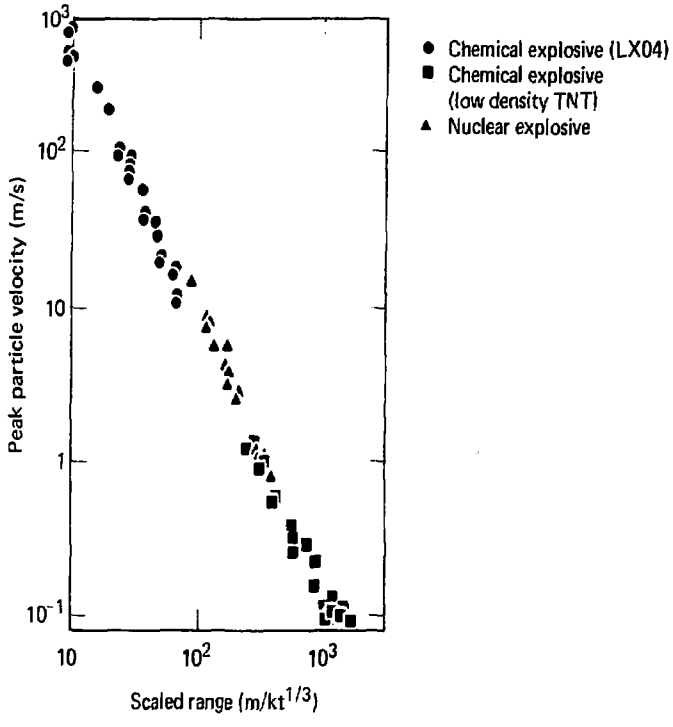

FIG. 14. Peak particle-velocity vs scaled range for chemical and nuclear explosions in salt: Larson's (1977a) small-scale high-explosive experiments (LX04), the Cowboy experiments (low-density TNT), and the Salmon experiment (nuclear explosive) (from Larson 1977b, and Trulio 1977).

Table 3 gives a summary of the conditions for transitions between the near and far fields for the three sets of peak-particle velocity data for explosions in salt (Fig. 14), together with estimates of observed dominant frequencies in the leading edge of the stress waves. Larson's (1977a) particle-velocity time histories in salt are similar to those shown in Figs. 7(a) and 9(a) with rise times from zero to peak particle-velocity that correspond to frequencies of approximately 10^5 to 10^6 Hz. A gauge record in Murphey's (1961) paper indicates a dominant frequency greater than 10 Hz for a tamped Cowboy explosion. A gauge record in Rogers's (1966) paper indicates a dominant frequency of about 5 Hz. These Cowboy and Salmon observations are consistent with Trulio's (1979) observation that the Salmon and Cowboy (scaled to Salmon) particle-velocity data are dominated by frequencies in the 1- to 10-Hz band. From Table 3, it appears

TABLE 3. Conditions for transition between the near and far fields for three sets of peak-particle velocity data near explosions in salt, and some observed dominant frequencies.

References	Experiments	Radial distance to gauge (m)	Approx transition freq (Hz)	Approx observed freq (Hz)
Larson (1977a)	Small-scale high-explosive	min: 0.04	1.6×10^4	$\approx 10^6$
		max: 0.14	4.7×10^3	$\approx 10^5$
Murphey (1961)	Tamped Cowboy high-explosive	min: 5.9	1.2×10^2	
		max: 178	3.8	>10
Rogers (1966), Patterson (1966)	Salmon nuclear-explosive	min: 168	4.1	
		253	2.8	≈5
		max: 744	9.2×10^{-1}	

that Larson's data are far-field data, the Salmon data are transition-field data, and the Cowboy data from the most distant gauge may be far-field data. These conclusions concerning the Salmon and Cowboy data are consistent with those of Trulio (1979). Trulio, after a careful examination of all the data, concluded that the Salmon data and most of the Cowboy data indicate nonlinear inelastic attenuation, and that the Cowboy salt may respond "elastically" at peak-particle velocities less than 0.04 m/s and peak radial stress values less than 4 bars (4×10^5 Pa). These low values of velocity and stress were measured on a "decoupled" Cowboy explosion in a mined cavity.

With respect to the rest of Larson's data summarized in Table 2, let us consider the wave forms illustrated in part(a) of Figs. 7-11. The rise times from zero to peak particle-velocity are approximately 1 μs, corresponding to frequencies on the order of 10^6 Hz for Westerly granite [Fig. 7(a)] and water [Fig. 10(a)]. Clearly, the radial decay exponents of 1.4 (water) and 1.5 (Westerly granite) represent inelastic stress-wave decay in the far field, and can be compared with the ideal elastic decay exponent of unity in the far field. This is also true for the observed decay exponents for Nugget sandstone (1.5), Blair dolomite (1.6), and Kemmerer coal (1.6). On the other hand, the dispersed wave forms for dry Mt. Helen tuff [Fig. 8(a)], saturated Mt. Helen tuff [Fig. 9(a)], and ice [Fig. 11(a)] have dominant frequencies of 10^4 to 10^5 Hz. In an ideal elastic version of the experimental assembly shown in Fig. 6, the near-field terms may not be negligible at these frequencies. Therefore, it may be that the attenuation exponents of 1.5 (dry Mt. Helen tuff at low stresses, and ice) and 1.9 (saturated Mt. Helen tuff) should be compared

with an ideal elastic radial decay exponent somewhat greater than unity. The same caution applies to the decay exponents for dry (1.6) and saturated (1.4) Indiana limestone, Tunnel tuff (2.1), and the frozen soils (2.0 and 2.7). A spectral analysis of the particle-velocity wave-form data would serve to resolve this near- vs far-field issue.

The conditions for the transition from inelastic to "elastic" response to stress waves are discussed further in Section 3.4.

3.3 Computer Calculations of Underground Explosions

Calculations with modern digital computers have been used in the study of underground nuclear explosions beginning with the first such explosion, Rainier (Johnson, Higgins, and Violet 1959). Computer calculations have been used to predict and interpret experimental measurements on explosions such as Salmon (Rogers 1966; Patterson 1966). They have been very useful in the prediction of inelastic effects for engineering applications of peaceful nuclear explosions (Cherry and Petersen 1970) and in the analysis of inelastic phenomena of importance in explosion containment (Terhune et al. 1977a,b). They are also useful in the study of explosions as sources of elastic seismic waves, but they have limitations for this application; the most serious limitation is discussed in this lecture.

Early examples of one- and two-dimensional codes for finite-difference calculations of elastic and inelastic stress-wave motion in solid materials are described by Wilkins (1964) and by Maenchen and Sack (1964). More recent descriptions of one- and two-dimensional codes used for underground explosion calculations at the Lawrence Livermore Laboratory are given by Schatz (1973, 1974) and by Burton and Schatz (1975). Similar codes have been developed and are being used by other organizations.

The above codes are based on a computational technique that identifies a finite number of material points and determines the motion in space-time and the physical state as a function of time of each point. This technique is the use of Lagrangian coordinates which are fixed in the material instead of being fixed in space as is the Eulerian system. The Eulerian and Lagrangian coordinate systems and the relations between them are described by Zel'dovich and Raizer [1966, Ch. I (1) 1-2]. The Lagrangian coordinates in a one-dimensional code correspond to a linear array of discrete points spaced along the radial coordinate axis. The Lagrangian coordinates in a two-dimensional code correspond to a two-dimensional array of discrete points in the plane defined by the longitudinal and radial axes of the cylindrical coordinate system.

The numerical solution for stress-wave propagation through a material is obtained by means of a step-by-step procedure through the feedback loop illustrated in Fig. 15 for each point (Lagrangian coordinate). The equation of motion (based on the fundamental equations for conservation of mass, linear momentum, and angular momentum) provides a functional relation between the applied stress and the acceleration of each point in the coordinate system. The energy conservation equation does not have to be used if there is no energy transport by heat conduction or radiation from one point to another; this is a valid approximation for stress-wave propagation in rock. However, the calculation of internal plus kinetic energy is useful in checking the accuracy of the calculation. The accelerations determined by the equation of motion are integrated over a discrete time interval (Δt) to obtain velocities; velocities are integrated over a discrete time interval (Δt) to obtain displacements; and displacements (relative to other point displacements), in turn, determine strains or deformations. The constitutive or state equations for the material give the relation between the applied strains and the resulting stress field. At the end of each cycle, time is incremented by $+\Delta t$ and the cycle is repeated.

There are several reasons for the present limitations of finite-difference computer calculations in the study of explosions as sources of seismic waves. The principal reason is discussed in this lecture: the constitutive or state equations relating strain and stress that have been developed do not model the inelastic response of rock with sufficient accuracy over the full range of the conditions generated by explosions.

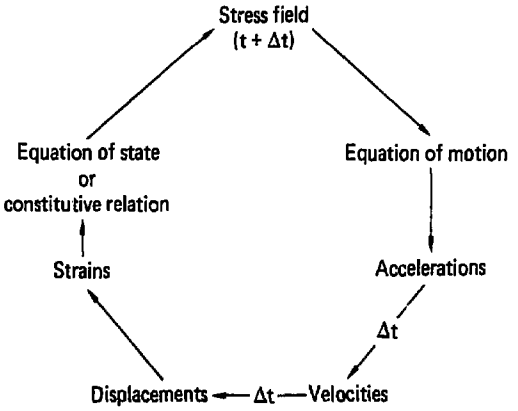

FIG. 15. Feedback loop for finite-difference calculations of stress-wave propagation (from Rodean 1971a).

The constitutive or state relations (hereafter called constitutive relations) are very simple in the case of linear, adiabatic, isotropic, elastic stress-wave propagation: the isentropic bulk modulus for compressional waves in a perfect fluid, and two moduli defined by the Lamé constants for compressional waves ($\lambda + 2\mu$) and shear waves (μ) in an ideal solid. The problem in calculating the explosion process, including the generation of seismic waves, is that of calculating the propagation of adiabatic stress waves that are initially nonlinear and inelastic, are attenuated by geometric and inelastic effects, and emerge from the explosion as almost-elastic or anelastic waves. The constitutive relations used in present computer programs or codes are very complex; but they approximately model only selected phenomena, not all aspects of stress-wave propagation. For example, let us consider the principal features of the constitutive relations for solids in the one-dimensional SOC73 code (Schatz 1973, 1974). (SOC73 also includes constitutive relations for liquid and gas phases and relations for solid-gas and solid-liquid phase transitions, but they are not considered in this lecture.) SOC73 is based as much as possible on known physical principles and measured rock properties, and as little as possible on nonphysical adjustable parameters.

Before discussing SOC73, it is appropriate to review some fundamentals of stress and strain in isotropic solid materials. The stress tensor Σ has nine components consisting of three normal (σ) and six shear (τ) stresses as shown in the first two terms of Eq. (8):

$$\Sigma = \begin{vmatrix} \sigma_{xx} & \tau_{xy} & \tau_{xz} \\ \tau_{yx} & \sigma_{yy} & \tau_{yz} \\ \tau_{zx} & \tau_{zy} & \sigma_{zz} \end{vmatrix} = \begin{vmatrix} \sigma_{rr} & 0 & 0 \\ 0 & \sigma_{\theta\theta} & 0 \\ 0 & 0 & \sigma_{\theta\theta} \end{vmatrix} . \tag{8}$$

There is a set of orthogonal axes, the principal axes of stress, along which the stresses are purely normal. In the symmetrical spherical coordinate system for an ideal spherical explosion, the stress tensor reduces to the third (right-hand) term in Eq. (8), where

$$\sigma_{\theta\theta} = \sigma_{\phi\phi}, \tag{9}$$

and the maximum shear stress is

$$\tau_m = (1/2)(\sigma_{\theta\theta} - \sigma_{rr}) = (1/2)(\sigma_{\phi\phi} - \sigma_{rr}). \tag{10}$$

The principal stresses can be written in terms of a mean normal stress (by definition, equal to the negative of the hydrostatic or

thermodynamic pressure) that determines uniform compression or dilatation,

$$-P = (1/3)(\sigma_{rr} + \sigma_{\theta\theta} + \sigma_{\phi\phi}), \tag{11}$$

and stress deviators that determine distortion,

$$\sigma_{rr} = -P + s_r, \tag{12}$$

$$\sigma_{\theta\theta} = -P + s_\theta, \tag{13}$$

$$\sigma_{\phi\phi} = -P + s_\phi. \tag{14}$$

From Eqs. (9)-(14),

$$s_r = -(4/3)\tau_m, \tag{15}$$

$$s_\theta = s_\phi = (2/3)\tau_m. \tag{16}$$

From these relations, it follows that the stress behavior of a material can be described in terms of a response to hydrostatic stresses and a response to shear stresses. Similarly, the strain can be described as a combination of volumetric strain and distortional strain (Jaeger and Cook 1971, Ch. 2.2, 2.4, 2.8, 2.12).

There are invariants of stress and of stress deviators that are independent of the orientation of orthogonal coordinates; it is obviously desirable to express criteria for material failure in terms of these invariants (Jaeger and Cook 1971, Ch. 2.4, 2.8). The stress invariants are, in spherically-symmetric coordinates,

$$I_1 = \sigma_{rr} + \sigma_{\theta\theta} + \sigma_{\phi\phi}, \tag{17}$$

$$I_2 = -(\sigma_{\theta\theta}\sigma_{\phi\phi} + \sigma_{\phi\phi}\sigma_{rr} + \sigma_{rr}\sigma_{\theta\theta}), \tag{18}$$

$$I_3 = \sigma_{rr}\,\sigma_{\theta\theta}\,\sigma_{\phi\phi}. \tag{19}$$

From Eqs. (11)-(19), the stress invariants can be written as

$$I_1 = -3P + J_1 = -3P, \tag{20}$$

$$I_2 = -3P^2 + 2J_1P + J_2 = -3P^2 + (4/3)\tau_m^2, \tag{21}$$

$$I_3 = -P^3 + J_1P^2 + J_2P + J_3$$

$$= -P^3 + (4/3)P\tau_m^2 - (16/27)\tau_m^3, \tag{22}$$

and the stress deviator invariants are defined as

$$J_1 = s_r + s_\theta + s_\phi = 0, \tag{23}$$

$$J_2 = -(s_\theta s_\phi + s_\phi s_r + s_r s_\theta) = (4/3)\tau_m^2, \quad (24)$$

$$J_3 = s_r s_\theta s_\phi = -(16/27)\tau_m^3. \quad (25)$$

Equations (20) and (23) are valid for all sets of principal stress axes, with appropriate substitutions for the subscripts r, θ, ϕ. The first two parts of Eqs. (21), (22), (24), and (25) are similarly valid for all sets of principal stress axes, but the third (right-hand) parts of these equations apply only to the principal stress axes of a spherically symmetric system as defined by Eqs. (8)-(10).

In SOC73 (Schatz 1974), it is assumed that the shear stresses do not affect the volumetric response of a material to changes in hydrostatic pressure, although it is known that this assumption is not correct. Shear stresses can enhance the compaction of a porous material under increasing hydrostatic loading. Shear stresses can also cause dilatation of a compacted material under increasing hydrostatic pressure. These effects are illustrated in Fig. 16. A modification of SOC was developed which included a

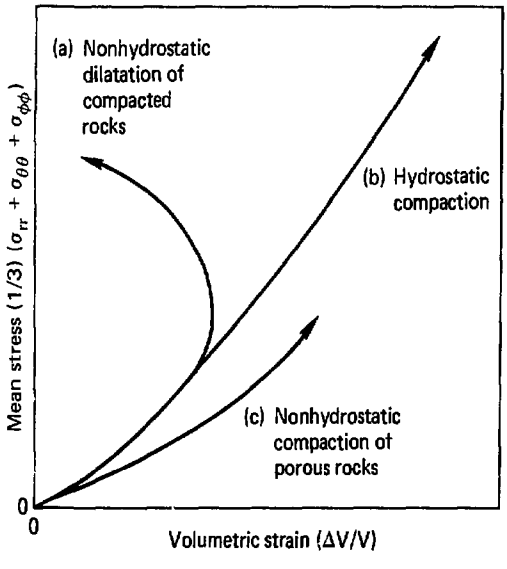

FIG. 16. Three types of quasi-static stress-strain response: (a) dilatation of compacted rocks under increasing nonhydrostatic stress, (b) compression under increasing hydrostatic pressure, and (c) shear-enhanced compaction of porous rock under increasing nonhydrostatic stress.

model for shear-enhanced compaction (Schatz et al. 1977), but the improved accuracy in modeling this aspect of rock deformation was not deemed to be worth the large increase of computer time required for a typical problem. SOC73 uses relations between hydrostatic pressure (P) and volumetric strain ($\Delta V/V$) that are based on laboratory measurements of stress and strain in rock samples. These stress strain relations are illustrated in Fig. 17 for nonporous and porous rocks. It is assumed that the material is incrementally elastic with a variable bulk modulus along each P vs $\Delta V/V$ curve; the shear modulus may be assumed to be constant or vary with the bulk modulus by assuming that Poisson's ratio is constant. If the rock is not porous, the loading and unloading curves are assumed to be identical; that is, there is no inelastic strain from hydrostatic stress, and there is no hysteresis in the P vs $\Delta V/V$ plane. If the rock is porous, the pores are crushed at sufficiently high pressures; this crushing is inelastic, and there is hysteresis because the inelastic strain is irreversible. The

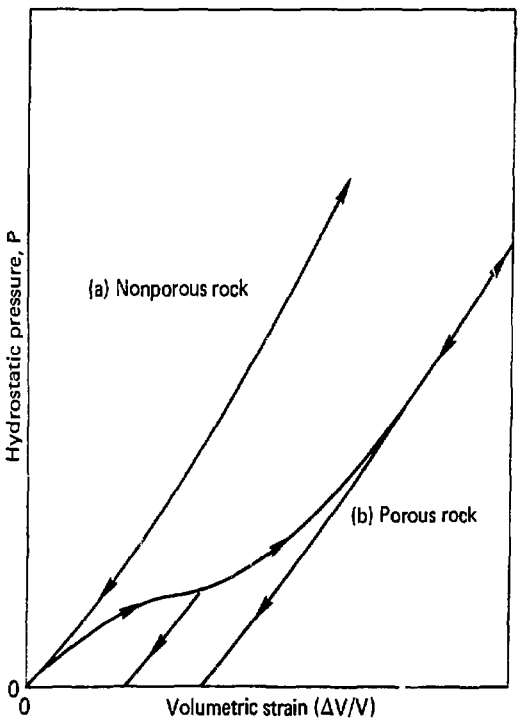

FIG. 17. Hydrostatic loading and unloading of (a) nonporous rock and (b) porous rock.

inelastic crushing of pores is very effective for dissipation of energy.

In SOC73, it is assumed that distortion in response to shear stress takes place at constant volume. The maximum shear strength of a material is a complex function of the applied stress. Cherry and Petersen (1970) found that the results of various destructive tests (compression, extension, and torsion) on glass, dolomite, limestone, and granite are quite consistent when plotted in terms of the second stress deviator invariant (J_2) vs a combination of the first stress invariant (I_1 or -P) and the third stress deviator invariant (J_3) as shown in Fig. 18. In the spherically-symmetric system implicit in SOC73, the invariant functions defining the coordinate axes in Fig. 18 can be simplified to the following, from Eqs. (9)-(16), (24), and (25):

$$|\tau_m| = |(1/2)(\sigma_{\theta\theta} - \sigma_{rr})| = |(1/2)(\sigma_{\phi\phi} - \sigma_{rr})| \qquad (26)$$

for the vertical axis, and

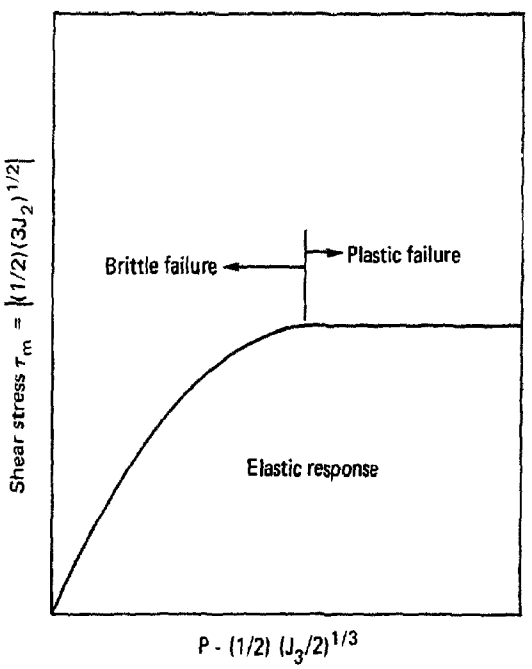

FIG. 18. Shear strength of rocks as a function of confining stress showing elastic response, brittle failure, and plastic failure.

$$P + (1/3)\tau_m = -(1/2)(\sigma_{rr} + \sigma_{\theta\theta}) = -(1/2)(\sigma_{rr} + \sigma_{\phi\phi}) \qquad (27)$$

for the horizontal axis. In SOC73, the maximum shear stess (τ_m) is limited to the values defined by an experimentally determined failure surface as illustrated in Fig. 18. If this maximum value of τ_m is reached at any Lagrangian coordinate, the material at that point is considered to have failed in shear, and a different failure surface for failed material is used for that material point during the remainder of the calculation. The transition between brittle and ductile failure in shear is defined as the condition at which increased loading ($P + (1/3)\tau_m$) does not result in an increase in shear strength (τ_m) as shown in Fig. 18. Strain hardening, which is observed in some materials, is not accounted for in SOC73.

In SOC73, tensile failure is defined as the state in which the shear-stress limit defined in Fig. 18 is reached and any principal stress is in tension. Tensile failure relaxes the tensile principal stresses while other principal stresses remain constant. As previously stated, shear failure relaxes the shear stress while the mean stress or hydrostatic pressure remains constant. Therefore, tensile failure affects the P vs $\Delta V/V$ relation while shear relaxation does not.

As stated in a preceding paragraph, SOC73 assumes no inelastic failure in the case of a nonporous material with identical loading and unloading paths in the P vs $\Delta V/V$ plane; consequently, there is no hysteresis for loading and unloading in this plane. However, there can be hysteresis in the σ_{rr} vs $\Delta V/V$ plane because of shear failure, as illustrated in Fig. 19. The difference between σ_{rr} and -P, for a given value of $\Delta V/V$, is equal to the value of the stress deviator [Eq. (12)], and the difference is limited by the shear strength of the material [Eqs. (24)-(27) and Fig. 18]. There would be no hysteresis in the σ_{rr} vs $\Delta V/V$ plane if there were no shear failure; the hysteresis loop in Fig. 19 is a consequence of irreversible deformation in shear and a corresponding dissipation of energy. Tensile failure would cause hysteresis in the P vs $\Delta V/V$ plane and possibly in the σ_{rr} vs $\Delta V/V$ plane.

As shown in the preceding paragraphs, the models in SOC73 for volumetric response to hydrostatic pressure, distortional response to stress deviators, and response to tension are based on simplified physical models and empirical relations fitted to experimental measurements on rocks. It is assumed in SOC73 that the relations between strain and stress in compression, shear, and tension are rate independent. Larson (1980a,b) and Larson and Anderson (1979a,b) conducted shock-wave studies on seven representative geological materials. They found time-dependent behavior in two highly porous rocks (dry and water-saturated tuff and limestone) and in one low-porosity rock (dolomite), but not in two

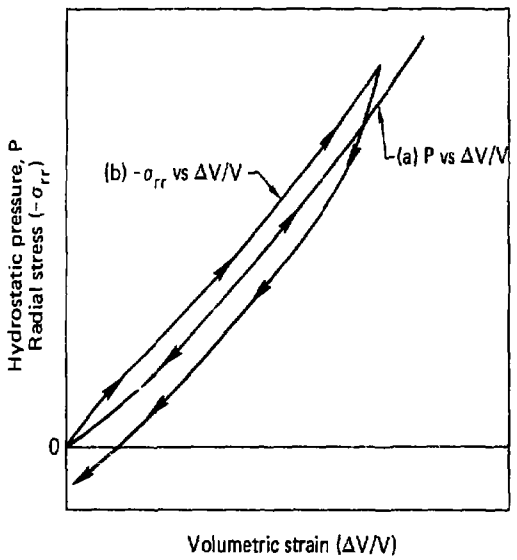

FIG. 19. Stress (P or $-\sigma_{rr}$) vs strain ($\Delta V/V$) loading and unloading cycles for (a) hydrostatic compression and dilatation, and (b) uniaxial compression and dilatation. Note the hysteresis loop in (b) because of shear failure.

other low-porosity rocks (granite and sandstone). Therefore, SOC73 cannot model the strain-rate effects that are observed in some rocks. However, SOC73 includes three strain-rate mechanisms that are required for the stability and accuracy of the finite-difference calculations. The first is the standard quadratic "artificial viscosity" developed by von Neumann and Richtmyer (1950) for finite-difference calculations of hydrodynamic wave propagation. This artifical viscosity acts to stabilize the calculations by "smearing" the shock-wave transition over several points along the radial Lagrangian coordinate axis. The second is a linear artificial viscosity that is equivalent to Voigt stress relaxation (low-pass filtering) that is a function of volumetric strain rate, and the third is equivalent to Maxwell stress relaxation (high-pass filtering) that is a function of shear or tensile strain rate. The Voigt model of a solid consists of a spring and a dashpot in parallel; the Maxwell model of a solid is composed of a spring and a dashpot in series (Jaeger and Cook 1971, Ch. 11.3). In shock compression and in shear or tensile failure, minimum values of these damping mechanisms are necessary for stable and accurate numerical computations. The quadratic

artificial viscosity rarely affects the physics implied by the numerical solutions for geological materials, but if the second (Voigt) and third (Maxwell) damping terms are greater than the required threshold values, they take on physical significance as rate-dependent constitutive terms. Viecelli (1973a) investigated the effect of the linear artificial viscosity or Voigt relaxation in TENSOR, a two-dimensional code that is similar in many respects to the one-dimensional SOC code. He found that the effect of the linear viscosity was viscoelastic attenuation of the peak particle velocity in a spherical compressional wave according to the relation expressed in Eq. (2)--$u \propto r^{-3/2}$.

Therefore, SOC73 does not give "elastic" stress-wave solutions, even if material failure does not occur in shear or tension. The linear viscosity (Voigt relaxation) is operative for all volumetric strain, even if shear or tensile failure requiring damping (Maxwell relaxation) does not occur. The Voigt relaxation time in SOC73 is selected for computational reasons, not for modeling observed anelastic or viscoelastic response.

From the above, it is clear that SOC73 calculations represent an approximation to the physical processes of stress wave propagation. SOC73 solutions for peak particle velocity or peak stress in the inelastic region can be fairly accurate if the stress-strain models are based on measured rock properties. However, SOC73 solutions for stress-wave time histories, particularly at low stress levels in the transition region between inelastic and almost-elastic response, are generally inaccurate if based on measured rock properties. SOC73 can be forced to give a good approximation to observations at a given gauge location in an experimental assembly, but the solutions for other gauge locations will probably be less accurate and the material properties implied in such forced solutions may be physically unrealistic. As noted in a preceding paragraph, the modeling in SOC73 could be modified to take more observed phenomena into account, but at the cost of increased code complexity and computation time. A comparison of measurements and calculations [with an earlier version of SOC (Cherry and Petersen 1970)] for the 5-kt Hardhat explosion is given in Rodean (1971a, Ch. 2.8); two illustrations are reproduced in Figs. 20 and 21.

Even if more complete descriptions of material response were incorporated into SOC73, there would still be substantial limitations to the accuracy of the calculated seismic source function for a given explosion. Geological inhomogeneities within the inelastic region of an explosion are more the rule than the exception. Even if the explosion site were "homogeneous," natural variability would introduce significant perturbations. Costantino (1978) conducted a series of 10 similar hydrostatic and triaxial compression experiments on samples from a single block of granite,

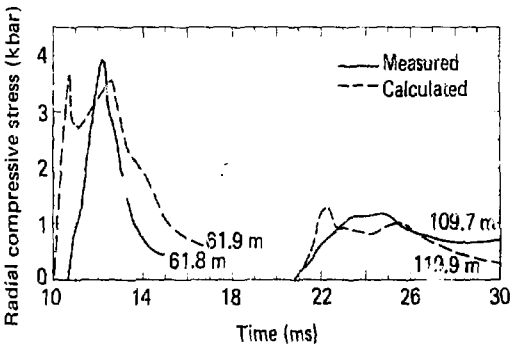

FIG. 20. Calculated and measured radial compressive stresses vs time for the 5-kt Hardhat explosion in granite (from Rodean 1971a).

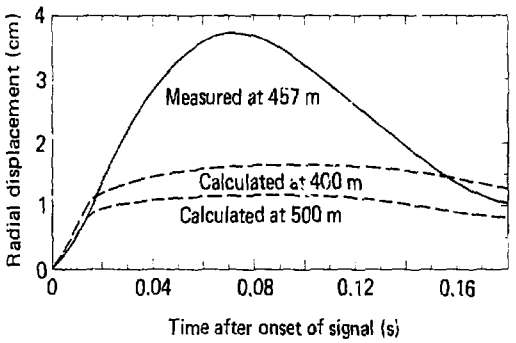

FIG. 21. Calculated and measured radial displacements vs time for the 5-kt Hardhat explosion in granite (from Rodean 1971a).

and concluded that a lower bound for experimental deviation for these physical property measurements in that material is about 20 percent in absolute volume strain.

3.4 Transition from Inelastic to "Elastic" Response

As previously stated, there is some ill-defined boundary called the "elastic radius" beyond which nonlinear inelastic deformation does not occur, but linear anelastic processes continue to attenuate the "elastic" waves from the explosion. The concept

of an elastic radius has been used since the beginning of "nuclear-explosion seismology." Werth, Herbst, and Springer (1962) used ground motion measurements near the first few underground nuclear explosions to define linear elastic-wave source functions. They combined these source functions with models of earth structure, linear anelastic attenuation, and instrument response to obtain synthetic seismograms that they compared with observations. They, and many later workers, made the simplifying assumptions that an explosion is spherical, that there is an "elastic radius" beyond which the stress-strain response is linear and almost-elastic, that measurements of ground motion beyond the elastic radius can be used to define an equivalent elastic source for the seismic waves generated by an explosion, and that linear attenuation functions can be used to model anelastic attenuation in the earth.

The term elastic radius implies that there is a distinct transition between nonlinear inelastic and linear elastic stress-strain response. Linear elasticity is a convenient and useful, but fictitious, concept. Linear anelasticity is a similar (perhaps fictitious) concept that is used in recognition of the truth that the response of the earth to seismic waves is not perfectly elastic. There has been disagreement as to whether seismic attenuation is nonlinear (Knopoff and MacDonald 1958) or linear (Savage and Hasegawa 1967). Recent experimental results (Brennan and Stacey 1977; Winkler, Nur, and Gladwin 1979) indicate that seismic attenuation in some rocks is linear at strains less than 10^{-6} and nonlinear at greater strains. As noted in Section 3.2, Trulio (1979) concluded that Cowboy salt may respond "elastically" at peak radial stresses less than 4 bars (4×10^5 Pa). For the Cowboy and Salmon salt properties given by Rogers (1966), this stress corresponds to a strain of about 10^{-5}.

In view of the above, it is proposed that the "elastic radius" marking the transition from nonlinear inelastic to linear elastic response be defined as the radial coordinate at which the strain from stress-wave propagation is 10^{-6}. This arbitrary definition could serve until a better one is established as a result of further research on the nature and existence of the transition from nonlinear to linear stress-wave response.

3.5 Reduced-Displacement Potential

The reduced displacement potential is a very useful seismic source function for a spherical wave in an ideal, infinite, homogeneous, isotropic, elastic solid. (Some investigators prefer the reduced-velocity potential, the time-derivative of the reduced-displacement potential. Each has its advantages. The reduced-displacement potential is directly related to the explosion moment [Eqs. (32)-(35)]. The reduced-velocity potential is proportional

to the far-field displacement [Eq. (30)] and its spectrum, as shown in Fig. 28, Section 5.3.)

The source of the spherical waves may be a finite spherical cavity with variable pressure or the limiting case of an infinitesimal point soure of dilatation (which may be approached by letting the cavity radius approach zero and the cavity pressure approach infinity in such a way that the product of the pressure and the cube of the radius remain constant and finite).

The first mathematical solution for elastic wave radiation from a spherical cavity was obtained by Jeffreys (1931) who assumed equal Lamé constants ($\lambda = \mu$) for the elastic solid. The first general solution in terms of λ and μ was obtained by Kawasumi and Yosiyama (1935). Blake (1952) and Selberg (1952) were the first to use the reduced-displacement potential in obtaining solutions for spherical wave propagation, but neither of them used that term for their source functions. Herbst, Werth, and Springer (1961) were the first to apply the term "reduced-displacement potential" to the potential function that is a solution of the spherical wave equation and is not a function of space but of reduced time alone.

Use of the reduced-displacement potential results in the following relation between the radial stress σ_{rr} (the driving function) and the reduced-displacement potential X (the response function):

$$\frac{\sigma_{rr}(r,\tau)}{4\mu} = \frac{1}{r^3}\left[(r/2\beta)^2 \frac{\partial^2 X(\tau)}{\partial \tau^2} + (r/\alpha)\frac{\partial X(\tau)}{\partial \tau} + X(\tau)\right], \qquad (28)$$

where the reduced time

$$\tau = t - (r - R)/\alpha, \qquad (29)$$

and

r = radial coordinate,
R = radius of cavity,
t = time,
α = compressional-wave velocity,
β = shear-wave velocity,
μ = shear modulus.

Selberg (1952) and Yoshiyama (1963) (apparently the Yosiyama of the Kawasumi and Yosiyama 1935 paper) derived equivalent forms of Eq. (28). The radial displacement (D_r) is related to the reduced-displacement potential as follows, where $X(\tau)$ is the input and $D_r(r,\tau)$ is the output:

$$D_r(r,\tau) = -\left[\frac{1}{\alpha r}\frac{\partial X(\tau)}{\partial \tau} + \frac{X(\tau)}{r^2}\right]. \tag{30}$$

The seismic moment for an earthquake was introduced by Aki (1966):

$$M_q = \mu S_q D_q, \tag{31}$$

where

D_q = average displacement in fault,
M_q = earthquake moment,
S_q = fault area.

Müller (1969) and Tsai and Aki (1971) extended the seismic moment concept to explosions and related the seismic moment to the reduced-displacement potential:

$$M_X(\tau) = 4\pi(\lambda + 2\mu)X(\tau) \tag{32}$$

where

λ = Lamé constant.

The final steady-state value of the reduced-displacement potential $[X(\infty)]$ is often used in defining the static value of the seismic moment of an explosion (Müller, 1973):

$$M_X = (\lambda + 2\mu) S_X D_X \text{ [note the similarity to Eq. (31)]} \tag{33}$$

where

$$D_X = X(\infty)/R_X^2, \tag{34}$$

$$S_X = 4\pi R_X^2, \tag{35}$$

and

D_X = radial displacement at reduced R_X in the elastic zone,
$R_X \geq$ "elastic radius" of explosion,
S_X = surface area of the sphere defined by the radius R_X.

Reduced-displacement potentials have been calculated from free-field ground-motion measurements by assuming spherical symmetry and that the ground motion at that gauge was elastic. Werth and Herbst (1963) published measured reduced-displacement potentials for nuclear explosions in alluvium, granite, salt, and tuff; Patterson (1966) for the Salmon explosion in salt; and Perret (1972a) for the Gasbuggy explosion in shale. Of these measurements, the best are those for Salmon and Gasbuggy because

these explosives were deeply buried; consequently the surface refection did not perturb the subsurface measurements until relatively late times. The ideal measurements of reduced-displacement potentials have never been made. Such ideal measurements would employ a large number of gauges in a low strain ($<10^{-6}$) region in which the stress-strain relation is most likely linear, below the explosion along ray-paths from the explosion to stations at teleseismic distances, and of high fidelity over the complete seismic spectrum from very short periods to final steady-state displacements.

4. CAUSES AND EFFECTS OF NONSPHERICAL GEOMETRY

In the preceding discussion, it is assumed that underground explosions are spherically symmetric. This assumption greatly simplifies the physics and mathematics of explosions, and it is a useful and valid approximation although all real underground explosions are nonspherical to some extent. In this lecture, we will consider two nonspherical aspects of underground explosions that are of importance in seismic monitoring: tectonic strain release and the effects of the free surface above the explosion.

4.1 Tectonic Strain Release

As mentioned earlier, geological and seismological evidence that some underground explosions released preexisting tectonic strain began to accumulate early in the history of underground nuclear testing. Two hypotheses have been advanced to explain this strain release. Press and Archambeau (1962) proposed that the strain release occurs around the inelastic fractured zone produced by the explosion (the tectonic strain field responds to the creation of a weak fractured zone around the explosion). The theory of this mechanism was developed further by Archambeau (1972). Brune and Pomeroy (1963) studied seismic data from the Hardhat explosion in granite. They concluded that the fractured zone hypothesis is not sufficient in the case of Hardhat, and that a dislocation was triggered on a nearby fault plane. They cited the occurrence of aftershocks as further support of the triggering hypothesis. Toksőz, Ben-Menahem, and Harkrider (1965) concluded that the fracture zone hypothesis is satisfactory for the Haymaker explosion in alluvium and the Shoal explosion in granite, but that the triggering hypothesis is required to explain the Hardhat observation. Archambeau and Sammis (1970) and Lambert, Flinn, and Archambeau (1972) concluded that the seismic data from the Bilby explosion in tuff and the Shoal explosion are consistent with stress relaxation around the fractured zone. Aki et al. (1969) considered both hypotheses in their study of the Benham explosion. They concluded that Benham triggered an earthquake, in part because the fracture zone hypothesis requires an unusually high

stress release in order to account for the observed Love wave from Benham. Aki and Tsai (1972) reviewed the Love wave data from 18 explosions in alluvium and tuff, and concluded that the evidence is in favor of the earthquake triggering mechanism. All explosions discussed in this paragraph were at the Nevada Test Site, except Shoal which was at another site in Nevada.

Even though there is disagreement about the mechanism of tectonic strain release by explosives, there is agreement on the usefulness of the parameter F that was introduced by Toksöz, Ben-Menahem, and Harkrider (1965), and has been used by Archambeau and Sammis (1970) and others. Toksöz, Ben-Menahem, and Harkrider defined F as the ratio of the strength of the earthquake-like source to that of the coincident explosion, but did not give an explicit mathematical definition. Hirasawa (1971) gave a mathematical definition of the parameter q that is the ratio of the strength of the double-couple component to the strengths of the explosion component of a composite seismic source. Müller (1973) found that Hirasawa's q is equal to the ratio of the moments of the earthquake and explosion components of a composite event; for example, in the static case,

$$q = M_Q/M_X, \tag{36}$$

where M_Q and M_X, are defined by Eqs. (31) and (33), respectively. Müller also gave a mathematical definition of the parameter F:

$$F = q\alpha^2/2\beta^2, \tag{37}$$

where

α = compressional-wave velocity,
β = shear-wave velocity.

Tectonic strain release is of interest at this Institute because it may make an underground explosion appear to be "earthquake like." Toksöz and Kehrer (1972) examined the seismic data for 28 underground nuclear explosions: 23 in the US and 5 (presumed) in the USSR. They estimated F ratios and the orientations of right-lateral, vertical, strike-slip faults that best fit the data. They found no evidence for tectonic release (F = 0) by three explosions: Sedan in alluvium, and Gnome and Salmon in salt. They determined F ratios greater than unity for only three explosions, all at the Nevada Test Site: Greeley (F = 1.6) in tuff, and Hardhat (F = 3.0) and Pile Driver (F = 3.2) in granite. They found no noticeable effect on the M_S:m_b discriminant in the case of these explosions. The north-northwest orientations of most of their fault plane solutions for explosions at the Nevada

Test Site are consistent with lineaments and fault planes in that area.

Toksöz and Kehrer also calculated surface-wave (Rayleigh wave) radiation patterns for composite sources as a function of F ratio, assuming vertical strike-slip faulting as the tectonic strain release mechanism. Patton (1980) made similar calculations in terms of the q ratio, but assuming dip-slip thrust faulting. Their results are compared in Table 4. As shown in this table, the effects on M_S of the two tectonic strain mechanisms are very different. The effect of a strike-slip mechanism is always positive as F is increased. In contrast, the effect of a dip-slip mechanism is first negative and then positive as q (or F) is increased. This difference in effect on M_S is a consequence of the different surface-wave radiation patterns produced by the two tectonic and the explosion mechanisms. The pattern from the explosion is circular, that from the dip-slip source is two-lobed, and that from the strikeslip is four-lobed. The phase angle of the pattern from the explosion differs by π (phase reversal) from the phase angles in both lobes in the pattern from the dip-slip source, so the interference between the explosion pattern and the dip-slip pattern is destructive. The phase angles of adjacent lobes in the four-lobed strike-slip pattern differ by π, so the interference between the explosive and tectonic pattern is alternately constructive and destructive. These mechanisms and their effects are also discussed in Harkrider's lecture at this Institute.

TABLE 4. Effect of tectonic strain release on magnitude. The calculations for the strike-slip case are by Toksöz and Kehrer (1972) and the dip-slip case are by Patton (1980). For Patton's calculations, $F \approx 1.5q$.

F	ΔM_S (strike-slip)	ΔM_S (dip-slip)	q
0	0	0	0
0.3	0.07		
0.5	0.08		
0.7	0.14	-0.4	0.5
1.0	0.24		
1.5	0.40	-0.4	1.0
2.0	0.53		
3.0	1.08	-0.1	2.0
4.0	1.23		
6.0		0.4	4.0
12.0		0.8	8.0

4.2 Effect of the Free Surface: Spall

The existence of the free surface above an underground explosion perturbs and distorts the spherical wave radiation from an explosion. An ideal spherical underground explosion radiates only compressional (P) waves. In a perfectly elastic half-space, these radiated P waves interact with the free surface and are converted into three types of elastic waves: reflected compressional (pP), vertically-polarized shear (SV), and Rayleigh (R or LR). In this lecture, we will consider the inelastic interaction of P and pP below the free surface (spall) and the possible effects of spall on compressional and Rayleigh waves from the combination of explosion and spall processes.

Spalling is a result of inelastic tensile failure of the rock that is caused by the conversion at the free surface of an upward-propagating compressional (P) wave into a downward propagating tensile (pP) wave. At some depth, the tensile stress in pP exceeds the sum of the compressional stress in P, the lithostatic stress, and the tensile strength of the rock. The tensile failure occurs at a time when the net momentum of the material above the fraction is upward. The spalled material then enters a ballistic trajectory that is terminated when the spall gap is closed. The net momentum of the spalled material is downward at the time of spall closure, and a downward impulse is applied to the underlying material. The seismic signals that may be generated by this impulse are of interest in the context of this Institute.

The spalling mechanism and its local mechanical effects are described in several publications. The dynamics of spalling by contained underground explosions have been investigated theoretically by Chilton, Eisler, and Heubach (1966). Spall measurements in several underground nuclear explosions have been analyzed by Eisler and Chilton (1964), Eisler, Chilton, and Sauer (1966), and Eisler (1967). Toman, Sisemore, and Terhune (1973) reported the spall measurements on the triple Rio Blanco explosion in Colorado and gave a preliminary interpretation of the data.

There have been studies (and speculations) concerning the possible relations between spall and distant seismic signals. Springer (1974) suggested that pP and a spall-closure (slap-down) phase (P_s) may contribute to the P wave and its coda at teleseismic distances. He reported estimates for the delay times corresponding to pP-P and P_s-P based on data from surface-zero accelerometers for a number of US underground nuclear explosions. A number of investigators had previously estimated pP-P delay times from teleseismic data, and Bakun and Johnson (1973) had estimated delay times for pP-P and P_s-P from teleseismic records from the Longshot, Milrow and Cannikin explosions in Amchitka. Springer found that his estimates for pP-P delay times agreed well

with those of the other investigators, but the agreement for P_S-P delay times was poor. Viecelli (1973b) conducted computer simulations of Rayleigh wave generation with and without spall. He found that the inelastic spall process generates larger amplitude Rayleigh waves than the purely elastic process. [Strictly speaking, Viecelli's "elastic" computations are for a viscoelastic medium because of the effect of the linear artificial viscosity that is necessary in finite-difference computations; see Section 3.3 on computer calculations and Viecelli (1973a).] Viecelli also noted that the spall-generated wave is delayed relatively to the elastically generated wave, but not as much as if the spall closure were the sole source of the Rayleigh wave. In addition, he noted that if spall closure were the sole source, the phase of the wave would be reversed relative to that of the elastically generated wave. His theoretical calculations, analytic and finite-difference, indicate that Rayleigh waves are generated by a combination of the elastic and spall-closure processes associated with an underground explosion. Viecelli also analyzed spall and regional Rayleigh wave measurements for underground nuclear tests at the Nevada Test Site, and concluded that the spall-closure impulse is sufficient to account for the amplitudes of the observed Rayleigh wave.

From the above, it appears that the inelastic process of surface spall has a more significant effect on Rayleigh waves than on teleseismic P and its coda. Furthermore, spall-closure is one of three contained underground explosion-related mechanisms that can generate Rayleigh waves that are reversed in phase at all azimuths, compared to the waves normally produced by buried explosions. The other mechanisms are cavity collapse [see Section 2.8 and Smith (1963)], and dip-slip tectonic strain release [see Section 4.1, Patton (1980), and Harkrider's lecture].

Murphy (1977) found that the observed long-period surface-wave data are inconsistent with a simple spherically symmetric source model, and suggested that the spall-closure phenomenon may be related to this discrepancy.

Rygg (1979) compared the Rayleigh waves from three presumed explosions of comparable magnitude in eastern Kazakhstan, and noted that the waves from one explosion were reversed in phase and delayed, relative to the waves from the other explosions. The event that generated the anomalous Rayleigh waves also excited very strong Love waves. Rygg considered three possible explanations for Rayleigh wave phase reversal. The explosion could have been so shallow that it acted as a downward-surface source, not a buried source; but a shallow source is not consistent with delayed Rayleigh waves. Cavity collapse could account for the delay and phase reversal, but not the observed Rayleigh wave amplitudes. Spall-closure could be consistent with the observed delay, phase

reversal, and amplitude of the observed Rayleigh waves. Rygg suggested that spall closure is the likely explanation. He did not consider dip-slip tectonic strain release. We may conclude that the role of spall closure in seismic signal generation has not been established with certainty.

5. FORWARD AND INVERSE PROBLEMS

This lecture, the other lectures on source theory, and the lectures on seismic wave propagation emphasize the forward problem. The forward problem may be defined by the question, "Given a seismic source, earth structure and properties, and a seismograph--what is the resulting seismogram at a given station?" The lectures on inversion theory and source classification emphasize the inverse problem. In question form, the inverse problem is, "Given a number of seismograms, the instrument characteristics, and the station locations--what is the earth structure; what are the earth properties associated with that structure; and (of principal interest at this Institute) what are the source location, origin time, and--especially--classification?" If the event is classified as an explosion, there is an additional question, "What was the yield?" In the remainder of this lecture, we will consider selected aspects of the forward and inverse problems in explosion seismology.

5.1 The "Equivalent Elastic Source": A Common Solution of the Forward and Inverse Problems

The physical models used in the numerical computations to obtain solutions for the forward and inverse problems are equivalent, but not necessarily identical. The numerical computations in the forward problem proceed in the same time and space directions as the physical processes being modeled, forward from the source to the receiver. The numerical computations in the inverse problem (if the data are inverted to obtain a solution) proceed backward in time and space from the receiver toward the source. The inverse problem can also be solved by trial-and-error: by making a series of forward-problem calculations for different combinations of system parameters.

In principle, the forward problem can be modeled from the detonation of the explosive to the recording of the seismogram. However, even if the conditions for a mathematically unique (and correct) solution from the data inversion obtain, the inverse problem can be solved only so far and no farther in space and time (hence the word "toward" in the next-to-last sentence in the preceding paragraph). The inverse problem can be solved by data inversion for linear, but not for nonlinear processes. The impenetrable barrier for data inversion is the so-called "elastic

radius" (more generally, the "elastic boundary") separating linear and nonlinear stress wave propagation. The data can be inverted to obtain a description of an "equivalent elastic source," but not of the nonlinear explosion processes. A solution for an "equivalent elastic source" can be unique in the mathematical sense, but the word "equivalent" means that this solution is not unique in the physical sense. This difference between the forward and inverse problems is illustrated in Fig. 22.

One "equivalent elastic source" is the reduced-displacement potential defined by Eqs. (28) and (29). As stated in Section 3.5, the reduced-displacement potential can be obtained experimentally by integrating the measured ground motion near an explosion. Two assumptions are implicit in reduced-displacement measurements: the ground motion is spherically symmetric and it is measured at a point where the stress-strain relation is linear and elastic. In reality, and at best, the ground motion is approximately spherically symmetric and linearly inelastic or anelastic. The reduced-displacement potential can be calculated

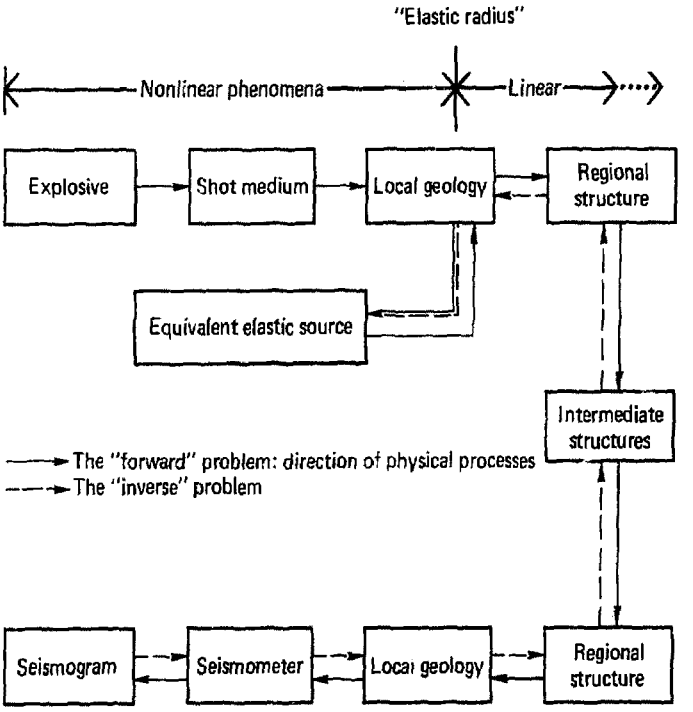

FIG. 22. Schematic diagram for the forward and inverse problems in seismology.

by finite-difference calculations of nonlinear and linear processes in an explosion (see Section 3.3 on computer calculations). The reduced-displacement potential can also be obtained from analytic solutions of Eq. (28) for a spherical cavity in an infinite elastic solid, with the cavity pressure (-P) replacing the radial stress (σ_{rr}). Therefore, in the context of the complete forward problem (source-propagation-receiver), the source component of the problem can be solved to obtain the "equivalent elastic source."

5.2 Comparison of Measured and Calculated (Forward Problem) Reduced-Displacement Potentials

In Fig. 21, the radial displacement measured at r = 457 m for the 5-kt Hardhat explosion in granite is compared with SOC calculations by Cherry and Petersen (1970) of the displacements calculated for r = 400 m and r = 500 m. The measured reduced-displacement potential at 457 m for Hardhat is compared in Fig. 23 with the reduced-displacement potential calculated for 500 m by Cherry and Petersen. Note that the measured peak displacement and measured peak reduced-displacement potential are greater than the calculated values, but that the agreement between measurement and calculation is much better at later times. Figure 24 compares measured and calculated (Cherry and Petersen 1970) radial displacements for the 29-kt Gasbuggy explosion in shale; Fig. 25 compares the measured and calculated reduced-displacement potentials. (The calculations were made for a yield of 25 kt.) Note again the significant difference between the peak values and the better agreement at later times. These figures illustrate that computer calculations, based on simplified models for stress-strain relations and measured rock properties, model some aspects of nonlinear inelastic and linear anelastic stress-wave propagation

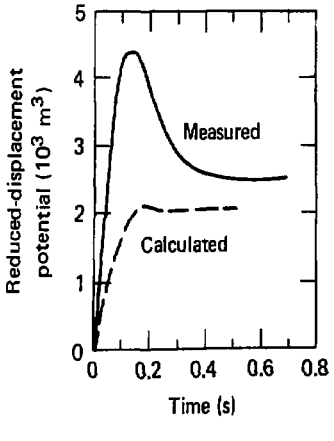

FIG. 23. Calculated and measured reduced-displacement potentials vs time for the 5-kt Hardhat explosion in granite (from Cherry and Petersen 1970).

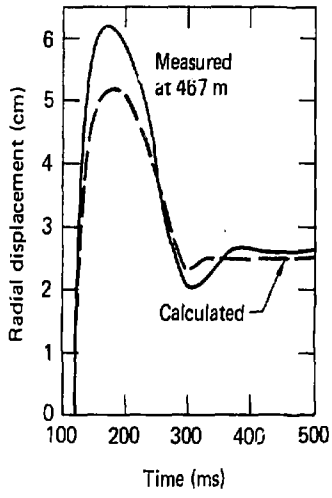

FIG. 24. Calculated and measured displacements vs time at a range of 467 from the 29-kt Gasbuggy in Lewis shale (from Cherry and Petersen 1970).

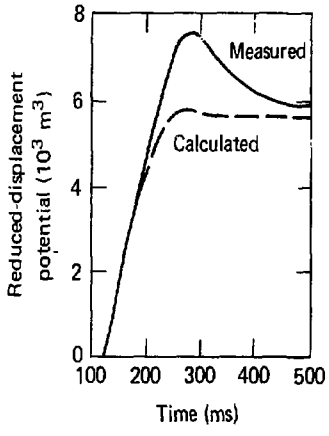

FIG. 25. Calculated and measured reduced-displacement potentials vs time for the 29-kt Gasbuggy explosion in Lewis shale (from Cherry and Petersen 1970).

better than others. The modeling appears to be better for the lower-frequency components of ground motion. As noted in Section 3.3, the accuracy of computer calculations could be improved by the use of more complete modeling of stress-strain relations, but at the cost of increased computer program complexity and computation time.

5.3 Analytic Solutions for the Reduced-Displacement Potential

Figures 26-28 illustrate some analytic solutions for the reduced-displacement potential (Rodean 1971a). Figure 26 shows

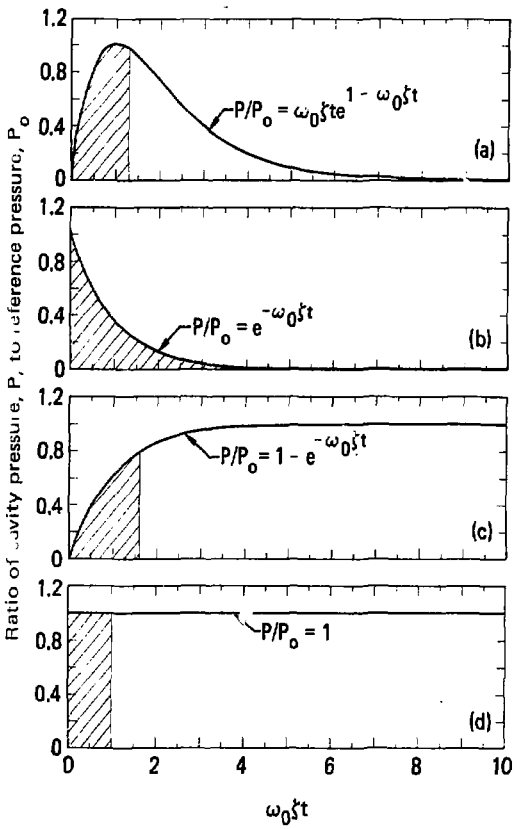

FIG. 26. Four special forms of the P-wave generating function. The hatched areas indicate equal impulse values (from Rodean 1971a).

four driving functions: (a) a cavity pressure function that initially increases linearly with time (t is dominant in the function) and then decays exponentially (exp $-\omega_0\zeta t$ is dominant), (b) a step in cavity pressure that immediately decays exponentially, (c) an exponential cavity pressure function that asymptotically approaches a constant value, and (d) a step change in cavity pressure. Functions (a) and (b) are impulse functions, and function (c) is a modified step function. The sum of the functions in (b) and (c) is equal to the function in (d). The parameters in Figs. 26-28 are defined as follows:

$$\zeta = \beta/\alpha = \text{damping ratio}, \tag{38}$$

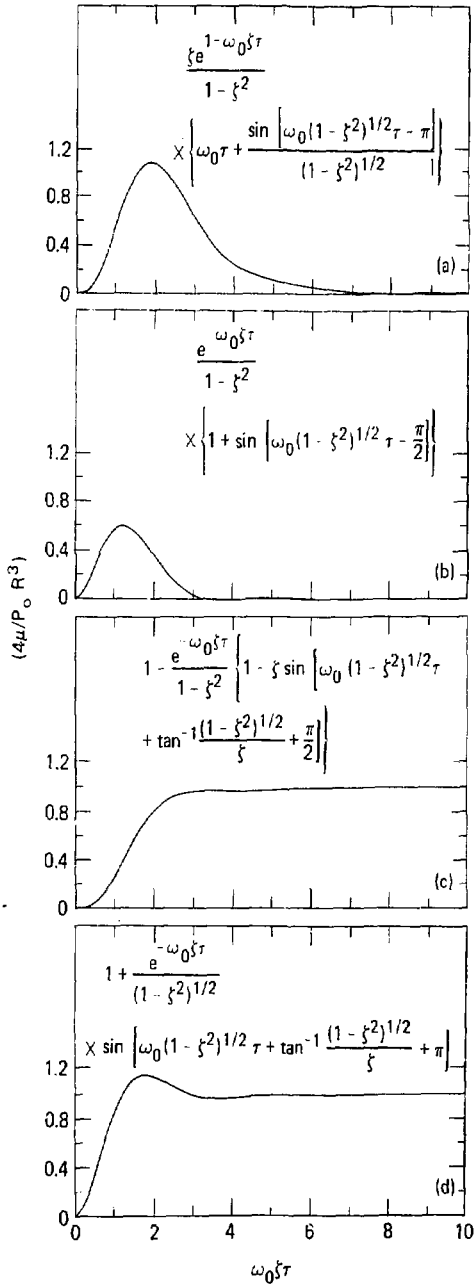

FIG. 27. Reduced-displacement potentials for the P/P_o vs time functions in Fig. 26 (from Rodean 1971a).

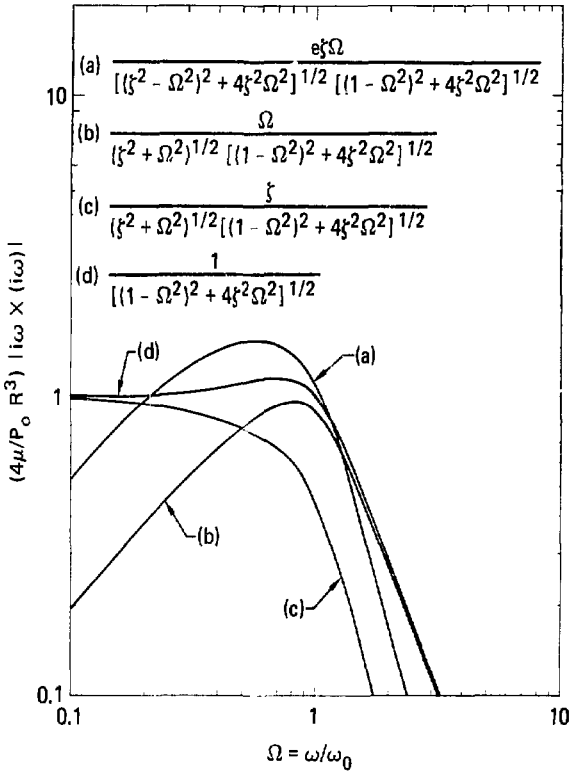

FIG. 28. Frequency response of an elastic medium to the P-wave generating functions in Fig. 26 (from Rodean 1971a).

$$\omega_0 = 2\beta/R = \text{characteristic undamped natural frequency,} \tag{39}$$

$$\Omega = \omega/\omega_0 = \text{dimensionless frequency.} \tag{40}$$

The parameters α, β, and R have the same identification as for Eqs. (28) and (29). Note that the final values of the reduced displacement potentials for the two impulse driving functions [Fig. 26(a) and (b)] are equal to zero [Fig. 27(a) and (b)], and that the final values for the two step driving functions [Fig. 26(c) and (d)] are nonzero [Fig. 27(c) and (d)]. Of the four driving functions in Fig. 26, only the two step functions result in permanent displacements or finite static moments [Eqs. (33)-(35)]. A comparison of Figs. 23, 25, 26(b) and 26(d) shows that the calculated reduced-displacement potentials for Hardhat and Gasbuggy may

be approximated by the reduced-displacement potential for a step change in cavity pressure, and that the measured reduced-displacement potentials are better approximated by a superposition of the reduced-displacement potentials for a pressure impulse plus a step change in pressure. Mueller and Murphy (1971) fitted impulse-plus-step functions of pressure to close-in free-field data for a number of underground nuclear explosions. The main point from the comparison of these figures is that an underground explosion with its inelastic processes can, for seismological purposes, be replaced by a spherical cavity in an elastic solid with an appropriate time-variation of cavity pressure.

5.4 Effect of the Driving Function on the Spectrum of the Reduced-Displacement Potential

The Fourier amplitudes of the time-derivative of the reduced-displacement potentials shown in Fig. 28 are proportional to the Fourier amplitudes of the far-field displacement [Eq. (30)]. The spectra for the driving functions illustrated in Fig. 26(a) and (c) (the two with an initial finite rate of cavity pressure increase) decrease at high frequencies in proportion to ω^{-3}. The spectra for the driving functions shown in Fig. 26(b) and (d) (the two with an initial step change in cavity pressure) decrease in proportion to ω^{-2} at high frequencies. The value of the exponent n in the function ω^{-n} has other physical significance. Hanks and Wyss (1972) showed that values of $n > 1.5$ are required in order that the energy radiated into the far field be finite. Randall (1973) discussed this further. He stated that the singularity in the time function with $n < 2$ would involve an infinite discontinuity in velocity, and that noninteger values of $n > 2$ would involve time functions with branch-point singularities which are not to be expected in physical situations. On the other hand, $n = 2$ corresponds to a singularity that has a finite jump in velocity. Randall did not mention it, but $n = 3$ implies a finite jump in acceleration, and acceleration is a continuous function if $n = 4$. Randall did state that there are sound theoretical reasons for expecting ω^{-2} behavior at high frequencies in seismic spectra.

There is another approach to approximating reduced-displacement potentials like those shown in Figs. 23 and 25. Haskell (1967) fitted a combination exponential-polynomial function of time to the four measured potentials of Werth and Herbst (1963). He required that displacement, velocity, and acceleration be continuous fuunctions of time, so the Haskell spectra are proportional to ω^{-4} at high frequencies. Von Seggern and Blandford (1972) relaxed this restriction, requiring that displacement be a continuous function in time, so their modifications of Haskell's spectra are proportional to ω^{-2} at high frequencies. They made this modification because the Haskell model did not match the

teleseismic data from the three explosions on Amchitka: Longshot, Milrow, and Cannikin.

5.5 Inverse Problem Solutions for Reduced-Displacement Potentials

A number of investigators have inferred equivalent elastic source time-functions from seismic data. Toksöz, Ben-Menahem, and Harkrider (1964) corrected observed Rayleigh-wave spectra for propagation effects to obtain source spectra. They found that the source spectra for two underground explosions and one cavity collapse at the Nevada Test Site are consistent with a cavity pressure function of the form $P = P_0\tau^{\xi}e^{-\eta\tau}$, with $\xi = 1$ and $\eta = 0.6$ for Sedan, $\eta = 1.0$ for Haymaker, and $\eta = 1.6$ for the Haymaker collapse. This pressure function is similar to that shown in Fig. 26(a). Subsequent investigators have favored trial-and-error solution of the inverse problem for the source function by assuming source functions and comparing synthetic with observed seismograms. Helmberger and Harkrider (1972) assumed a reduced displacement potential function of the form $X = X_0\tau^{\xi}e^{-\eta\tau}$, and found that the long- and short-period data from the Boxcar explosion fit this function for $\xi = 0.5$ and $\eta = 0.15$. Von Seggern and Blandford (1972) found that Mueller and Murphy's (1971) model, based on close-in free-field data, with its ω^{-2} high-frequency characteristic, fit the teleseismic P-wave data from Longshot, Milrow, and Cannikin on Amchitka better than Haskell's (1967) model with its ω^{-4} high-frequency characteristic. They removed the quartic and cubic terms from Haskell's model and adjusted parameters in the resultant exponential-polynomial function of time to approximate the reduced-displacement potentials given by the Mueller-Murphy impulse-plus-step function for cavity pressure. Aki, Bouchon, and Reasenberg (1974) compared observed Rayleigh waves from underground nuclear explosions in the US with synthetic seismograms for different source models. They found that a Haskell/von Seggern-Blandford reduced-displacement potential, modified for ω^{-3} high-frequency behavior and for considerable overshoot in the time domain, was required to match synthetic with observed seismograms. Peppin (1977) proposed a very different model based on local and regional observations of the Jorum and Handley explosions: a combination of an upward impulse and a spherical dilatation source. The spectrum of his spherical source has no overshoot at the corner frequency ($\omega = \omega_0$ in Fig. 28) and is proportional to ω^{-3} or ω^{-4} at high frequencies. Burdick and Helmberger (1979) modeled short- and long-period P waves at teleseismic distances from events on Amchitka and Novaya Zemlya. They commented that there are problems with pressure and potential functions of the form $\tau^{\xi}e^{-\eta\tau}$ (there is no steady-state component consistent with cavity formation, and the far-field functions have singularities at $\tau = 0$). They used a von Seggern-Blandford reduced-displacement potential modified to give considerable overshoot (corresponding to a step-function plus a considerable

impulse for the cavity-pressure function in the Mueller-Murphy model) in matching synthetic seismograms with observations. The results of these investigations are summarized in Table 5.

There is no general consensus among the above papers, and the discrepancies among interpretations of observations that Müller (1973) noted still exist. Burdick and Helmberger (1979) made important criticisms of the $\tau^{\xi} e^{-\eta\tau}$ functions used by Toksöz, Ben-Menahem, and Harkrider (1964), and Helmberger and Harkrider (1972): these source functions tend toward zero at late times, and they have singularities in the far field at $\tau = 0$ (also see the footnote to Table 5 concerning values of ξ). This leaves the step-plus-impulse functions of cavity pressure (Mueller and Murphy 1971) and the reduced-displacement potentials of the form

$$e^{-\eta\tau} \cdot \left[\sum_{n=0}^{n} a_n \tau^n \right]$$

where η and a_n are adjustable parameters, and $n = 4$ (Haskell 1967), $n = 3$ (Aki, Bouchon, and Reasenberg 1974), or $n = 2$ (von Seggern and Blandford 1972; Burdick and Helmberger 1979). Since the von Seggern and Blandford model can be made to closely approximate the Mueller-Murphy model, the two models may be considered to be equivalent. There is disagreement about the required far-field high-frequency displacement spectrum: ω^{-2} (Mueller and Murphy; von Seggern and Blandford; Burdick and Helmberger), or ω^{-3} (Aki, Bouchon, and Reasenberg; Peppin 1977). There is disagreement about overshoot in the reduced-displacement potential: none (Peppin), moderate (Mueller and Murphy; von Seggern and Blandford), considerable (Aki, Bouchon, and Reasenberg; Burdick and Helmberger), or infinite (Toksöz, Ben-Menahem, and Harkrider; Helmberger and Harkrider). Peppin alone proposes a nonspherical source: an upward impulse superimposed on a spherical source of dilatation.

It is clear that more research is needed to resolve the discrepancies among the explosion source models obtained from solutions of the inverse problem. The high-frequency part of the displacement spectrum and the overshoot are discussed further in subsequent sections.

6. DETECTION, IDENTIFICATION, AND YIELD ESTIMATION

We will now apply the preceding material to seismic monitoring; specifically, the problems of detection, discrimination, and estimating the yields of explosives. We have not discussed the effects of explosion yield, except in connection with the scaling of experimental measurements to a common yield (see Figs. 5 and

TABLE 5. Equivalent elastic-source functions based on observations.

Reference	Data	Function	Far-field high-frequency characteristics
Toksoz, Ben-Menahem, and Harkrider (1964)	Rayleigh waves	$P(\tau) = P_0 \tau e^{-\eta\tau}$	ω^{-3}
Mueller and Murphy (1971)	close-in free-field	$P(\tau) = P_0 + P_1 e^{-\eta\tau}$	ω^{-2}
Helmberger and Harkrider (1972)	Rayleigh and P waves	$X(\tau) = X_0 \tau^{1/2} e^{-\eta\tau}$	-[a]
von Seggern and Blandford (1972)	P waves	$X(\tau) = f_1(e^{-\eta\tau}) \cdot f_2(\tau, \tau^2)$	ω^{-2}
Aki, Bouchon, and Reasenberg (1974)	Rayleigh waves	$X(\tau) = f_1(e^{-\eta\tau}) \cdot f_2(\tau, \tau^2, \tau^3)$	ω^{-3}
Peppin (1977)	Rayleigh and P waves	$X(i\omega)$ flat to corner plus upward impulse	ω^{-3} perhaps ω^{-4}
Burdick and Helmberger (1979)	Long- and short-period P waves	$X(\tau) = f_1(e^{-\eta\tau}) \cdot f_2(\tau, \tau^2)$ with overshoot	ω^{-2}

[a]The noninteger value of the exponent for τ makes the mathematics difficult. In their Appendix C, Gardner and Barnes (1942) list Laplace transforms only for functions of $\tau^n e^{\eta\tau}$ with $\eta = -1$, $\eta = 0$, and $\eta =$ positive integers.

7-14). A key question that we will now try to answer is, "What are the effects of yield on explosion phenomena and related seismic observations?" Or, in other words, "What are the scaling rules for the seismic effects of explosions?" In trying to answer these questions, we will also have to consider the effects of depth of burial and the properties of the explosion medium.

6.1 Detection: Effect of Explosion Environment

Given the capabilities of a seismic net for detecting events at a given location, the principal variables that determine the probability that an explosion will be detected are its yield and the seismic-coupling properties of the surrounding medium. In this section, we consider seismic coupling.

Underground nuclear explosions are a very inefficient means of generating seismic energy. The ratio of the radiated seismic-wave energy to the explosion yield, the seismic-coupling efficiency, is very low for such explosions. As noted in the section on thermal effects, postshot analysis of rock temperatures indicates that 90 to 95 percent of the energy released by contained underground nuclear explosions is deposited as residual thermal energy (Heckman 1964; Rawson, Taylor, and Springer 1967; Edwards and Holzman 1968). Mueller (1969) analyzed close-in free-field and local seismic measurements of ground motion from six underground nuclear explosions: four tamped, one cratering, and one in a decoupling cavity. (Decoupling is discussed in a subsequent paragraph.) The seismic-coupling efficiencies of these explosions, as determined by Mueller, are given in Table 6. Perret (1972b) analyzed close-in free-field ground-motion measurements for 21 contained underground nuclear explosions. His results, in terms of seismic-coupling efficiencies for different rock types, are given in Table 7. Mueller's results show significant seismic coupling differences among contained, cratering, and decoupled explosions. Perret's results illustrate the effects of rock properties on seismic coupling, consistent with the data for explosions in different types of rock in Figs. 5 and 7-14. For a given yield, the seismic signals from an explosion in granite, rhyolite, or salt are much stronger than those from an explosion in dry porous rocks like alluvium or tuff.

The low seismic-coupling efficiency of underground explosions is illustrated by the following simplified model of an underground explosion: a step change in pressure in a spherical cavity in a homogeneous, isotropic, infinite elastic solid. The seismic-coupling efficiency of this system is (Rodean 1972):

$$E_S/E_X = 3(\bar{\gamma} - 1)P/8\mu, \qquad (41)$$

where

E_s = radiated seismic wave energy,
E_x = explosion energy,
P = step change in cavity pressure,
$\bar{\gamma}$ = ratio of enthalpy to internal energy of cavity gas,
μ = shear modulus of elastic solid.

P is limited by the shear strength of the elastic solid, and $\bar{\gamma}$ is a function of the cavity gas composition and temperature. It can be shown (Rodean 1972) by means of Eqs. (8)-(16) that the cavity pressure change is limited to

$$P \leq (8/3)|\tau_m|, \tag{42}$$

TABLE 6. Seismic-coupling efficiencies of underground nuclear explosions determined by Mueller (1969).

Explosion	Type	Medium	Seismic-coupling efficiency (%)
Shoal	Contained[a]	Granite	1.8
Salmon	Contained	Salt	5.8
Boxcar	Contained	Rhyolite	4.6
Benham	Contained	Tuff	6.1
Schooner	Cratering[b]	Tuff	0.32
Sterling	Decoupled[c]	Salt	0.0084

[a]Contained in this table also means "tamped"; that is, the explosive assembly was in close proximity to the surrounding rock.

[b]A Peaceful Nuclear Explosion.

[c]A contained explosion in the cavity formed by the Salmon explosion.

TABLE 7. Seismic-coupling efficiencies of contained underground nuclear explosions determined by Perret (1972b).

Environment	Seismic-coupling efficiency (%)
Alluvium, dry	0.05 to 0.15
Tuff, dry	0.10 to 0.30
Tuff, wet	2 to 3
Shale, deep	2
Dolomite	2
Granite	2
Ryolite	2
Salt, dome	3

where τ_m is the shear strength defined in Fig. 18. From Eqs. (41) and (42), the upper limit for seismic-coupling efficiency is

$$E_S/E_x = (\bar{\gamma} - 1)\tau_m/\mu. \tag{43}$$

For representative values of $\bar{\gamma}$ for the cavity gas and measured values of τ_m and μ, Eq. (43) gives seismic efficiencies consistent with the data in Tables 6 and 7 (Rodean 1972). Equations (41) and (42) can also be used in the analysis of cavity decoupling.

The concept of cavity decoupling was introduced by Latter et al. (1961). Herbst, Werth, and Springer (1961), reporting the results of the Cowboy experiments in a salt mine with high explosives, showed that seismic signals are significantly reduced in amplitude if the explosions are detonated in a sufficiently large cavity. Springer et al. (1968) reported the results of the 380-t Sterling nuclear explosion in the cavity produced in a salt dome by the 5.3-kt Salmon explosion. The Sterling reduced-displacement potential, scaled to the Salmon yield, indicates a decoupling ratio of 70 ± 20 at 1 to 2 Hz. That is, the Fourier amplitudes at 1 to 2 Hz of the Salmon reduced-displacement potential are 70 ± 20 times those of the Sterling reduced-displacement potential, scaled to the Salmon yield. The basic reason why decoupling works is illustrated in Fig. 5: the inelastic explosion-produced stress wave attenuates more rapidly to a lower stress level in air (the strong-shock solution) than in rock (Rodean 1971b).

Patterson (1966) made calculations of fully- and partially-decoupled explosions in salt. (Full decoupling occurs when the cavity walls respond elastically to the explosion; partial decoupling when the walls respond inelastically.) He did not make enough calculations to satisfactorily define the transitions from full decoupling through partial decoupling to tamped explosions. Terhune, Snell, and Rodean (1979) made a series of calculations to define these transitions. They studied the seismic-coupling efficiency of nuclear explosions in granite by means of computer calculations as a function of scaled explosion source radius. The scaled-source radii were varied from 0.1 $m/kt^{1/3}$ (point source) to 20 $m/kt^{1/3}$ (a nearly full-decoupling cavity). They found that seismic coupling efficiency is at a maximum when the scaled-source radius is approximately 2 $m/kt^{1/3}$. The primary cause of this maximum seismic-source strength is the effect of initial source radius on peak-particle velocity and the pulse duration of the outgoing elastic wave. A secondary cause is that rock vaporization (an energy sink) does not occur for scaled-sourced radii greater than 1 $m/kt^{1/3}$. Therefore, for scaled-source radii greater than 1 $m/kt^{1/3}$, there is additional energy available for seismic wave generation. Available data from underground nuclear

explosions at the Nevada Test Site do not provide sufficient evidence to either support or negate the enhanced coupling that is indicated by calculations at scaled-source radii of 1 to 2 m/kt$^{1/3}$. The final (steady-state) value of the calculated reduced-displacement potential as a function of scaled initial cavity radius is shown in Fig. 29. Figure 30 shows the final energy balance (among the cavity gas, rock fractures, and seismic waves) as a function of scaled initial cavity radius.

From the above, it is clear that changes in explosion environment can change the seismic signal amplitude from an explosion of given yield by factors of approximately 10 (variations in geology) to 100 (cavity decoupling). This corresponds to changes of 1 to 2 units of seismic magnitude. Therefore, the detection of an explosion by a seismic network is strongly dependent upon the environment in which the explosive is emplaced.

6.2 Seismic Scaling Rules for Underground Nuclear Explosions

We will now address seismic scaling rules for nuclear explosions in a given medium. Examples of cube-root of the yield scaling are given in Figs. 5 and 14 (m/kt$^{1/3}$) for experimental

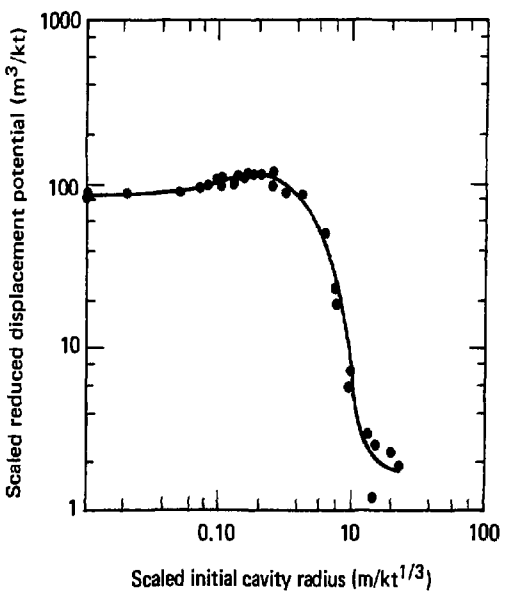

FIG. 29. Final reduced-displacement potential vs scaled initial source radius (from Terhune, Snell, and Rodean 1979).

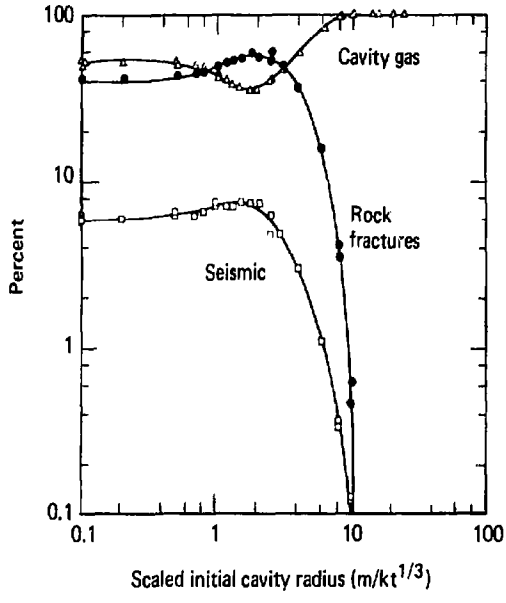

FIG. 30. Final energy balance vs scaled initial source radius (from Terhune, Snell, and Rodean 1979).

measurements of explosions with different yields. The rationale for cube-root scaling is based on the spherical symmetry of an explosion. During the explosion, the average energy density varies in inverse proportion to the volume enclosed by the outward-propagating spherical stress wave. Different explosion effects are associated with different energy densities: rock vaporization, rock melting, rock fracture, transition at the "elastic radius" from nonlinear inelastic to linear anelastic stress-wave response, etc. Therefore, the characteristic lengths of an explosion, such as the "elastic radius," in a system with explosion yield as the only independent variable, are proportional to the cube-root of the reciprocal of energy density: $m/kt^{1/3}$. It is assumed that gravity has no effect; its actual effect is considered in a subsequent paragraph.

In Fig. 27, four normalized solutions for reduced-displacement potentials are presented, and the corresponding normalized spectra of the time-derivatives of these potentials are shown in Fig. 28. The normalizing factor for the potentials is $(4\mu/P_0R^3)$ and for the frequency, from Eqs. (39) and (40), is $(2\beta/R)$. In Figs. 27 and 28, and in Eq. (39), R is the radius of a cavity in an elastic

medium and P_o is a reference cavity pressure. For an underground nuclear explosion with yield Y, $R = R_x$ is the "elastic radius" and $P_o = P_x$ is the negative of a reference radial stress. With P_x constant, the scaled "elastic radius" is

$$R_s = R_x/Y^{1/3}, \tag{44}$$

the scaled undamped natural frequency is

$$\omega_s = 2\beta/R_s, \tag{45}$$

and the normalizing factor for the reduced-displacement potentials is $(4\mu/P_x R_s^3)$. The units of R_x are $m/kt^{1/3}$. There was considerable interest in seismic-scaling rules for underground nuclear explosions in the early days of underground testing because there had been only a few tests, the yields of these tests were low, and there were few seismic measurements. For example, during 1957-1958 there were only five underground nuclear tests at the Nevada Test Site for which seismic magnitudes were determined; the yield of these explosions ranged from 55 t to 19 kt [see Table 7.1 in Rodean (1971a)]. One of the best early papers on the subject of seismic-scaling rules, worthy of study today because of its treatment of fundamentals, is by Carpenter, Savill, and Wright (1962). They critically review the cube-root scaling rule and some variations. They show that body-wave amplitude vs yield curves are strongly dependent upon the seismic source spectrum and the seismometer characteristics, especially narrow band vs broad band. Werth and Herbst (1963) used cube-root scaling of measured reduced-displacement potentials for explosions in alluvium, granite, salt, and tuff to calculate theoretical regional headwave (P_n) amplitude vs yield curves, taking anelastic attenuation in the earth and instrument response into account. Carpenter (1967) extended this work of Werth and Herbst to P waves at teleseismic distances, and included P-wave amplitude vs yield curves from scaled source functions for underwater and near-surface atmospheric explosions. Rodean [see Ch. 7.5 in Rodean (1971a)] calculated similar regional P_n- and teleseismic P-wave amplitude vs yield curves for the four reduced-displacement potentials shown in Figs. 27 and 28. Springer and Hannon (1973) used cube-root scaling to develop teleseismic P-wave amplitude vs yield relations for different source functions. In all the above work, the reduced-displacement potentials were cube-root scaled without considering possible depth of burial effects. In general, the theoretical body-wave amplitude vs yield curves obtained by the above authors are, in log-log coordinates, nonlinear over a yield range from 1 to 10^3 kt, with slopes of about unity at low yields and "turnover" to lesser slopes at high yields, as shown in Figs. 31 and 32 for P_n and teleseismic P-waves. This "turnover" is a consequence of the shift of the source spectrum (see Fig. 28) toward lower frequencies [see Eqs. (39), (40), (44), and (45)] as

yield increases. The instrument bandpass is centered at about 1 Hz, so the seismometer samples the lower frequencies of a low-yield spectrum (relative to the corner frequency ω_o) and the higher frequencies of a high-yield spectrum. Note in Figs. 31 and 32 that the earth-attenuated peak displacement is nearly linear with yield (in log-log coordinates) even if the seismometer response to the displacement is not.

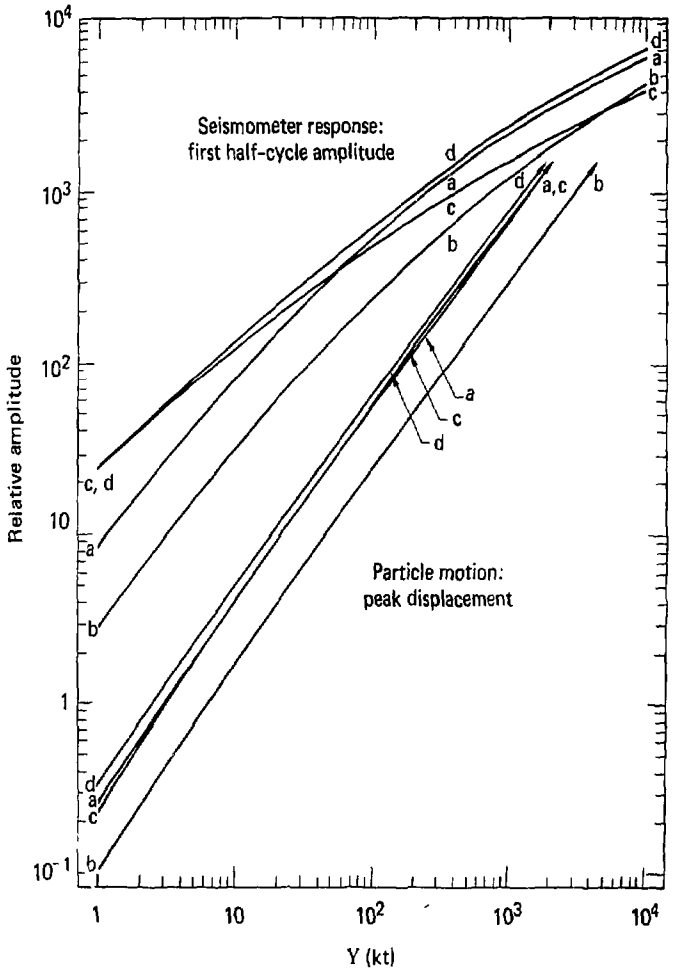

FIG. 31. Regional amplitude-yield curves: attenuated-head-wave particle motion and seismometer response at 680 km. Curves a,b,c, and d are based on applied-stress functions of Fig. 26 a,b,c, and d (from Rodean 1971a).

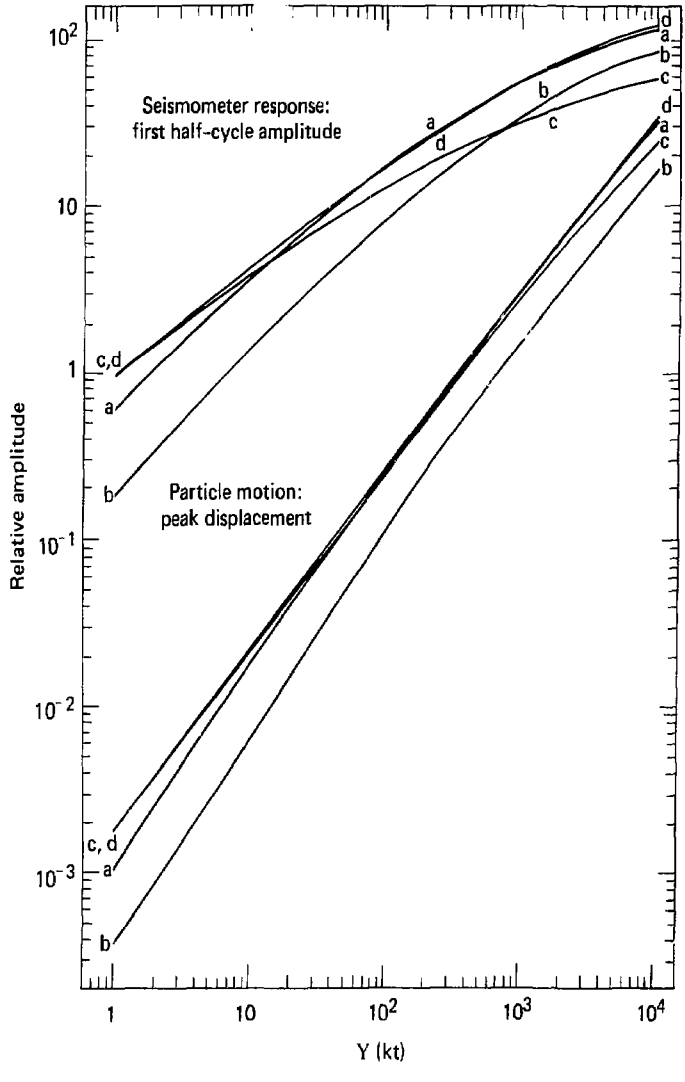

FIG. 32. Teleseismic amplitude-yield curves: attenuated-body-wave particle motion and seismometer response at 3400 km. Curves a,b,c, and d are based on applied-stress functions of Fig. 26 a,b,c, and d (from Rodean 1971a).

After a decade or so of underground testing, there were sufficient data to derive statistical relations for magnitude vs yield for yields ranging from about a kiloton to a little over a megaton. Ericsson (1971) developed the statistical theory for linear magnitude vs log yield ($\log_{10}$ Y) relations, considered the magnitudes to be expected from given yields, and the yields to be expected for given magnitudes. He demonstrated his approach with teleseismic m_b and M_s data from a network of Canadian stations for six tests with announced yields in the Pahute Mesa testing area at the Nevada Test Site. Marshall, Douglas, and Hudson (1971) proposed linear M_s vs log yield relations, one for consolidated and one for unconsolidated rocks, based on data for 31 explosions with announced or presumed yields in the US, Algeria, and the USSR (20 were at the Nevada Test Site). Basham and Horner (1973) analyzed teleseismic body and surface-wave data from a Canadian network for 3 explosions on Amchitka, 32 in the continental US (28 at the Nevada Test Site), 4 presumed explosions in eastern Kazakhstan, and 6 presumed explosions on Novaya Zemlya. They developed linear m_b and M_s vs log yield relations based on announced and presumed yields for US explosions. Springer and Hannon (1973) used data from several networks at regional and teleseismic distances for 17 explosions in the Pahute Mesa testing area of the Nevada Test Site to develop the equivalent of m_b and M_s vs log yield relations. The slopes of the m_b and M_s vs log yield relations for explosions in rhyolite and tuff at the Nevada Test Site determined in three of these investigations are summarized in Table 8.

The linear m_b and M_s vs log yield relations that Ericsson (1971), Basham and Horner (1973), and Springer and Hannon (1973) developed from statistical analysis of observations are not consistent with the nonlinear theoretical scaling relations that Werth and Herbst (1963), Carpenter (1967), Rodean (1971a), and Springer and Hannon (1973) based on cube-root scaling with yield

TABLE 8. Slopes of linear magnitude vs log yield relations for explosions in tuff and rhyolite at the Nevada Test Site.

		Teleseismic m_b		
Reference	Regional m_b	Short-period	Long-period	M_s
Ericsson (1971)		0.93		1.19
Basham and Horner (1973)		1.09	0.72	1.23
Springer and Hannon (1973)	0.63	0.99		1.09

of reduced-displacement p ntials. Mueller and Murphy (1971) developed a cube-root sca g rule modified to include empirical depth-of-burial effects. hy (1977) showed that the modified Mueller-Murphy scaling rule is consistent with the Springer-Hannon relations for short-period P-wave data at regional and teleseismic distances, and with the Basham-Horner relations for short- and long-period P-waves data at teleseismic distances. However, the Mueller-Murphy scaling rule is not consistent with the Springer-Hannon and Basham-Horner relations for long-period surface waves. Murphy concluded that these data are not consistent with a simple, spherically symmetric model. He suggested that this discrepancy may be related to the spall-closure phenomenon.

The underground explosion effects are superimposed upon the underground environment, including the lithostatic or overburden pressure. Some constitutive relations between stress and strain, like rock vaporization from shock compression and unloading, may be assumed to be independent of the overburden pressure associated with underground explosions. Others, such as the stress-strain relation for the transition from nonlinear-inelastic to linear-anelastic response, may be strongly affected by overburden pressure. Therefore, the radius of vaporization may be expected to vary with the cube-root of the explosion yield, but the "elastic radius" may be expected to vary in proportion to the cube-root of the yield and some inverse function of the overburden pressure. The final value of the reduced-displacement potential or the static moment of the explosion [Eqs. (32)-(35)] may be a function of the final cavity volume. According to containment analysis calculations, the final dynamic cavity pressure can vary between one-third to twice the initial overburden pressure, depending upon the mechanical properties of the rock (Terhune et al. 1977a). The mechanical properties of a given type of rock can vary significantly from site to site; therefore the explosion-produced cavity volume per kiloton at a given depth can vary from site to site. The French nuclear explosions in a granite massif in Algeria formed cavities with scaled volumes (in cubed metres per kiloton) that averaged about one-fifth the average scaled volumes of cavities produced by US nuclear explosions in granite rocks in Nevada (Gauvenet 1970). The scaling relation for these explosions in Algeria included the effect of rock strength as well as depth of burial (Michaud 1968). Computer calculations based on quasi-static rock strength measurements indicate that the relative absence (Algeria) or presence (Nevada) of water in preexisting fractures may be responsible for this difference in scaled cavity size (Rodean 1972). On the other hand, dynamic experiments with shock waves do not indicate any loss of shear strength because of the presence of water in Westerly granite (Larson and Anderson 1979b). Therefore, for a given set of rock properties, the final value of the reduced-displacement potential may be proportional to the yield and some inverse function of the overburden pressure.

From data obtained at the Nevada Test Site, Mueller and Murphy (1971) give the following respective empirical relations for the cavity radius (R_c) and the "elastic radius" (R_x) as functions of yield and overburden pressure (ρh):

$$R_c \propto Y^{0.29}\rho^{-0.24}h^{-0.11}, \tag{46}$$

$$R_x \propto Y^{1/3}(\rho h)^{-0.42}, \tag{47}$$

where

h = depth of burial,
ρ = average overburden density.

As noted by Mueller and Murphy (1971), yield and depth of burial are generally not independent variables at the Nevada Test Site because of testing practice for containment. For most explosions at that location,

$$h \propto Y^{1/3}. \tag{48}$$

Geological properties (e.g., porosity, water content, strength, etc.) that affect R_c and R_x are also a function of depth. Therefore Eqs. (46) and (47) implicitly describe the variation of R_c and R_x with the overburden effect of depth and with other parameters [material properties and, per Eq. (48), yield] that also vary with depth. From Eqs. (46)-(48),

$$R_c \propto Y^{0.25}\rho^{-0.24}, \tag{49}$$

$$R_x \propto Y^{0.19}\rho^{-0.42}. \tag{50}$$

Equation (49) is essentially identical with the theoretical scaling rule that includes the effects of gravity (Chabai 1965):

$$R_c \propto (Y/\rho)^{1/4}. \tag{51}$$

Springer and Denny (1976) studied the broad-band velocity spectra of the complete regional wave trains from about 40 events at the Nevada Test Site. Their spectra therefore contain considerable information about the regional earth structure as well as the source. They found that the "corner frequency" is almost independent of yield, and noted a tendency for it to vary inversely with approximately the sixth power of the yield. From Eqs. (39) and (40) and Fig. 28, this implies that $R_x \propto Y^{1/6}$; this is close to the Mueller-Murphy relation in Eq. (50).

According to Eqs. (40) and (50), the ratio R_x/R_c decreases as yield and depth increase, which is physically reasonable. As a consequence of these and other equations, the impulse component of

the Mueller-Murphy step-plus-impulse pressure functions (see Table 5) increases relative to the step component as yield and depth increase. Similarly, this overshoot in the time-and-frequency domains of the reduced-displacement potential increases with yield and depth. It is this increase in overshoot with yield and depth that makes this source model approximate the long- and short-period teleseismic body-wave magnitude vs yield observations of Basham and Horner (1973), and the short-period regional and teleseismic body-wave magnitude vs yield observations of Springer and Hannon (1973). This increase of overshoot with yield and depth is in contrast to the effect of depth on finite-difference calculations of the reduced-displacement potential of an explosion. In such calculations, the overshoot increases with decreasing depth because of the decrease in shear strength with decreasing overburden pressure (see Fig. 18).

In summary, cube-root scaling is suitable for high-stress phenomena in the central part of the explosion, but not for seismic source definition if depth is a variable. In particular, cube-root scaling does not give results that are consistent with magnitude and yield data. The Mueller-Murphy modification of cube-root scaling gives significantly better results for body-wave magnitude vs yield, but not for surface-wave magnitude vs yield. No existing spherically symmetric explosion-scaling model accounts for all observed magnitude vs yield data. Clearly, there is need for further work on the effects of yield, depth, and material on seismic source parameters.

6.3 Body vs Surface-Wave Magnitude Relations for Underground Nuclear Explosions

Most of the available unclassified yield data for underground nuclear explosions are for explosions at the Nevada Test Site, and most of the explosions at this location have been in alluvium and volcanic rocks (tuff and rhyolite). For example, Marshall, Springer, and Rodean (1979) list announced or presumed yields for 46 underground nuclear explosions. Of these, 29 were at the Nevada Test Site, and 26 of the 29 were in alluvium or volcanic rocks. The Mueller-Murphy model is based, for the most part, on data from explosions in alluvium and volcanic rocks at this site. One way to extend the geological and geographical data base for underground nuclear explosions is to study the body- vs surface-wave magnitude data for announced and presumed underground nuclear explosions in different parts of the world.

In analyzing m_b:M_S data, Liebermann and Pomeroy (1969) and Basham (1969) noted that the m_b:M_S data for explosions and earthquakes in the western United States are anomalous with respect to such data for the Aleutians, Algeria, and the USSR. Marshall and Basham (1972) confirmed that the m_b:M_S relations

for explosions in the western US differ from those for explosions in the Aleutians, the USSR, and China, but they did not detect any regional differences in m_b:M_s data for earthquakes. This is illustrated in Fig. 33 for explosions at the Nevada Test Site, in the Aleutians, and in the USSR. There is an offset and a different slope for the m_b:M_s relations for the two populations: explosions at the Nevada Test Site, and explosions in the Aleutians and the USSR. Marshall, Springer, and Rodean (1979) developed an empirical correction to the body-wave magnitude for anelastic attenuation in the upper mantle, and incorporated this correction in a new body-wave magnitude, m_Q. The explosions of Fig. 33 are plotted in terms of m_Q vs M_s in Fig. 34. It is shown that the change from m_b to m_Q reduces the offset of the two populations, but there is still a difference in slope. The present question is, "What is the reason for the difference between the m_Q vs M_s slope for explosions at the Nevada Test Site and the slope for explosions in the USSR?" (The two explosions on Amchitka don't have much effect on the statistics.)

Marshall (1979) has suggested that the different slopes for the two populations of explosions are a consequence of different

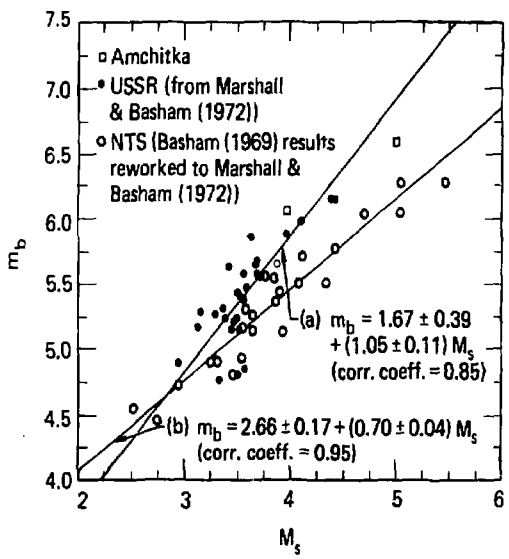

FIG. 33. Plot of m_b vs M_s for underground nuclear explosions in North America and the USSR. Line (a) is for Amchitka and Soviet explosions, line (b) is for Nevada Test Site explosions (from Marshall, Springer, and Rodean 1979).

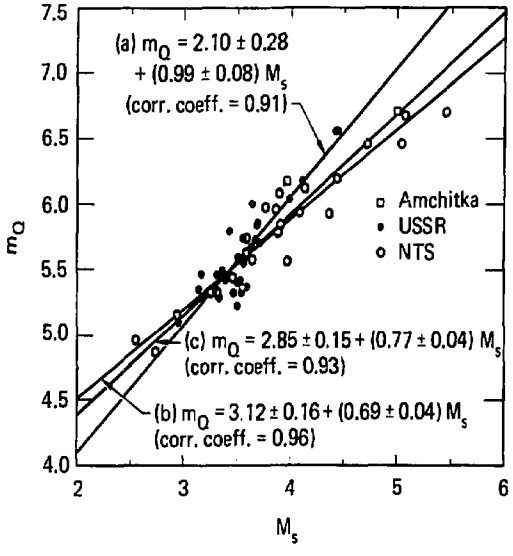

FIG. 34. Plot of m_Q vs M_S for underground nuclear explosions in North America and the USSR. Line (a) is for Amchitka and Soviet explosions, line (b) is for Nevada Test Site explosions, and line (c) is for all the explosions shown (from Marshall, Springer, and Rodean 1979).

slopes for the m_Q vs log yield relations and a common M_S vs log yield relation for the two populations. Figure 35 is from Marshall, Springer, and Rodean (1979). The top m_Q vs log yield relation is for selected explosions on Amchitka, the Panute Mesa, and Yucca Flat testing areas at the Nevada Test Site, and peaceful nuclear explosions (PNEs) in the US. The bottom relation is for explosions in salt and granite and for PNEs in India and the USSR. Figure 36, also from Marshall, Springer, and Rodean, gives a common M_S vs log yield relation for almost all the explosions in Fig. 33. In Table 9, magnitude vs log yield relations from Figs. 35 and 36 are used to derive m_Q vs M_S relations that are compared with the m_Q vs M_S relations from Fig. 34. The comparison of (d) with (e) and of (f) with (g) in Table 9 illustrates Marshall's hypothesis that the difference between the body-wave seismic coupling characteristics of (1) the younger volcanic rocks at Amchitka and the Nevada Test Site, and (2) salt, granite, and older consolidated rocks in the USSR is responsible for the different m_Q vs log yield and m_Q vs M_S relations shown in Figs. 31-34. Data for more explosions in salt, granite, and old

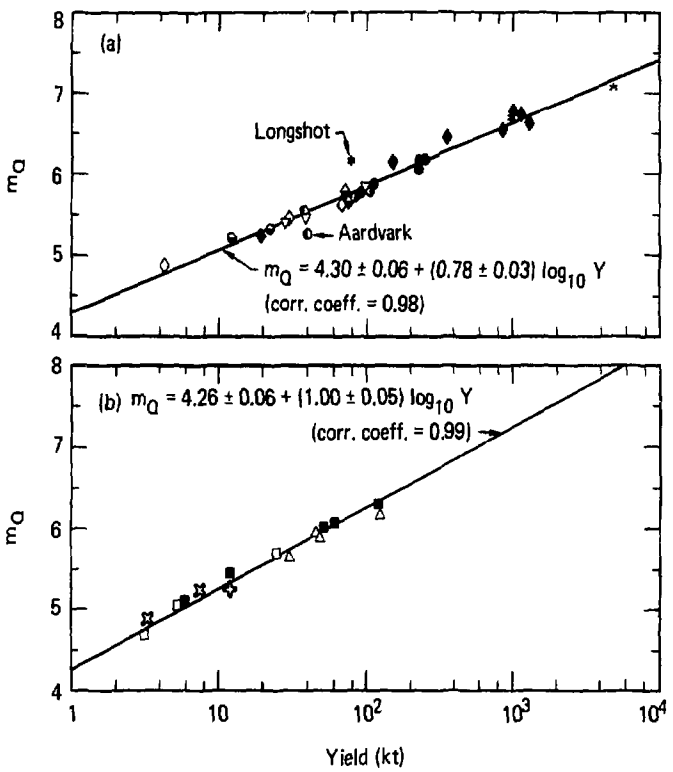

- Amchitka
- Pahute below water table
- Pahute above but close to water table
- Pahute above water table

Yucca

- Below water table
- Above but close to water table
- Above water table, high water content
- Above water table, in or close to Paleozoic

Medium

- Salt
- Granite-nuclear
- Granite-chemical at Medeo; plotted at twice chemical yield

PNEs

- US
- India
- USSR

FIG. 35. Plots of m_Q vs yield for selected explosions: (a) at Amchitka, Pahute Mesa, and Yucca Flat at the Nevada Test Site, and PNEs in the Western US; and (b) in salt and granite, and PNEs in India and the USSR. The Medeo explosions (high-explosive) were not included in calculating the line in (b) (from Marshall, Springer, and Rodean 1979).

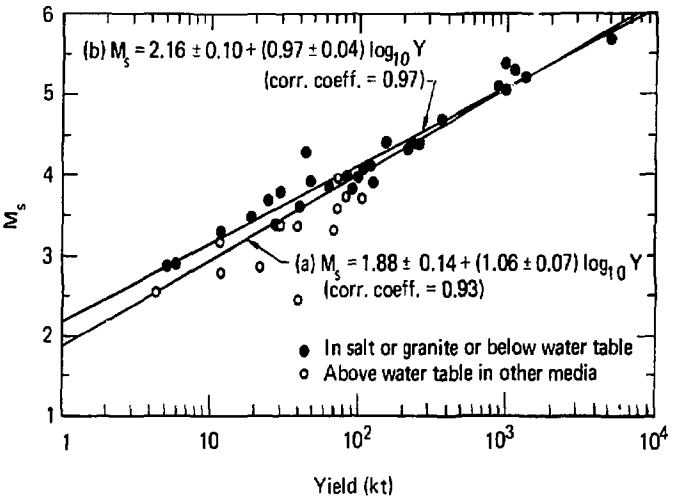

FIG. 36. Plot of M_S vs yield for selected nuclear explosions. Line (a) gives the result for all the explosions shown, and line (b) gives the result for the explosions in salt or granite or below the water table (from Marshall, Springer, and Rodean 1979).

consolidated rocks would be invaluable in confirming or negating Marshall's hypothesis.

6.4 Identification: Effects of Inelastic Processes on Signal Composition, Duration, and Spectra

In the two preceding sections, especially Section 6.2, the emphasis is on scaling explosion phenomena from low to high yields. Much of this emphasis is a consequence of history--the first underground tests were at low yields, and the effects to be expected at high yields were of considerable interest. High-yield explosions have provided considerable seismic data for source descriptions (Section 5.5), magnitude-yield relations (Section 6.2), and the m_b:M_S discriminant (Section 6.3). The identification of a strongly-coupled (Section 6.1) high-yield explosion is relatively simple because seismic data are generally available from a large number of stations. Identification can be difficult for low-yield explosions, especially if they are weakly coupled or decoupled (Section 6.1), because limited seismic data may be available from only a few stations. Detection by a few stations not only reduces the amount of data, but also introduces the problem of magnitude overestimation (Ringdahl 1976) which Christofferson will discuss in his Institute lecture. Therefore,

TABLE 9. Summary of empirical m_Q vs log yield, M_S vs log yield, and m_Q vs M_S relations from Marshall, Springer, and Rodean (1979).

No.	Fig.	Relation	Comments
a	35	$m_Q = 4.30 + 0.78 \log_{10} Y$	*Amchitka: volcanic;* Nevada Test Site: volcanic; western US: sandstone and shale
b	35	$m_Q = 4.26 + 1.00 \log_{10} Y$	US: salt and granite; Algeria: granite; India: sandstone; USSR: clay, salt, and sandstone
c	36	$M_S = 2.16 + 0.97 \log_{10} Y$	All of the above
d	34	$m_Q = 2.10 + 0.99 M_S$	Amchitka, USSR
e	-	$m_Q = 2.03 + 1.03 M_S$	From (b) and (c)
f	34	$m_Q = 3.12 + 0.69 M_S$	Nevada Test Site
g	-	$m_Q = 2.86 + 0.80 M_S$	From (a) and (c)

the emphasis in scaling for purposes of identification should be in scaling from high-yield explosions (which can be exhaustively analyzed) to low-yield explosions (which can be similarly analyzed only if there are extensive local and regional seismic measurements). In Section 6.2 it is noted that yield and depth are generally not independent variables because of testing practices for containment. Clandestine tests, the object of seismic monitoring under a comprehensive test ban, may be expected to be buried at greater than standard depths. Therefore the effects of depth and yield must be separated in scaling data from high-yield explosions to low-yield explosions for seismic identification purposes.

The principal inelastic phenomena in an underground nuclear explosion are associated with cavity formation and the generation of the outward-propagating approximately spherical P wave. As a result of local geological inhomogeneities, no real explosion is perfectly spherical and some S-wave energy is also directly radiated. For explosions with yields of a few kilotons, the inelastic processes associated with the direct-P and direct-S wave generation are completed in 0.1 to 0.2 second. This is the time required for cavity formation (Johnson, Higgins, and Violet 1959;

Rogers 1966), and the radial displacement transient in the almost-elastic zone is completed in a similar time interval (Figs. 21, 23-25). According to the hypothesis that tectonic strain release occurs outside the inelastic fractured zone around the cavity (Archambeau 1972), tectonic strain release is coincident in space and time with the explosion. According to the triggering hypothesis (Brune and Pomeroy 1963; Aki and Tsai 1972), the fault displacement may be triggered outside the immediate vicinity of the shot point. Such tectonic strain release is not coincident in space with the explosion; it may not be coincident in time but delayed a few seconds [e.g., the delayed Rayleigh waves observed by Rygg (1979)]. Spall failure can occur less than a second after detonation, and spall closure can occur 1 to 3 seconds after detonation (Springer 1974). Therefore the principal inelastic processes that are associated with the generation of the main seismic signal from a low-yield explosion (inelastic deformation around the cavity, triggered fault motion, spall closure) are fractional-second processes that take place within a few seconds. Cavity collapse and aftershocks usually generate seismic waves that are distinct from the principal seismic signal.

The explosion is an approximately spherical process; therefore the direct seismic radiation consists of compressional-wave energy and some small fraction of shear-wave energy. Other shear waves are generated by reflection and refraction of compressional waves at the free surface and at interfaces between layers in the local geological formations. Rayleigh waves are generated by interaction of the direct seismic radiation with the free surface. As noted in Sections 4.2 and 6.2, spall closure may make a significant contribution to the generation of Rayleigh waves. Tectonic strain release is associated with perturbations in the Rayleigh-wave radiation pattern and with Love wave generation. The principal differences between explosions and earthquake spectra are at the long periods associated with Rayleigh and Love waves. The reason that the m_b:M_s discriminant works is probably because the primary radiation from explosions is mostly compressional waves. Primary radiation from earthquakes has a much larger fraction of shear-wave energy, and shear waves are more efficient in generating Rayleigh waves than are compressional waves.

6.5 Yield Estimation: Effects of Seismic Coupling Efficiency and Signal Attenuation

Linear magnitude vs log yield relations have been empirically determined for underground nuclear explosions, as noted in Section 6.2. One must make two assumptions in applying such relations developed for one test site to estimate the yields of explosions at another site: the seismic coupling efficiency is approximately

the same at both locations, and the signal propagation characteristics from both sites to their respective receiving networks are comparable. As noted in Section 6.1, variations in geological properties around the shot point can cause as much as 1 seismic-magnitude-unit variation for explosions of a given yield. Regional variations in attenuation in the upper mantle can cause magnitude variations to vary from 0.1 to 0.3 units; Marshall, Springer, and Rodean (1979) developed an empirical magnitude correction for this effect. Seismic yield estimates for explosions at a given site can therefore have a significant systematic mean error (or bias) as well as random errors about the mean (Ericsson 1971; Basham and Horner 1973; Marshall, Springer, and Rodean 1979).

We will use seismic yield estimates by Dahlman and Israelson (1977) to illustrate systematic mean errors and random errors about the mean. They used announced yields for 16 explosions in tuff and rhyolite in the Yucca Flat and Pahute Mesa testing areas of the Nevada Test Site to develop a single linear source function vs log yield relation. [The magnitude vs log yield relations for explosions in saturated tuff and rhyolite in these testing areas are essentially identical (Marshall, Springer, and Rodean 1979)]. They used this relation in estimating the yields of 178 explosions at the Nevada Test Site. They assumed that the coupling of explosions in tuff is three times that of explosions in alluvium. They used the tuff-rhyolite relation for explosions in other media (granite, dolomite, limestone). They did not make any corrections for explosion depth, moisture content of the shot media, or the depth of the static water table.

Their yield estimates (Y_e) were compared with the official explosion yields (Y_o) by Rodean (1979). The statistical distributions of the ratios of the estimated to the official yields are shown in Figs. 37-39 for explosions in the Yucca Flat, Pahute Mesa, and Rainier and Shoshone Mesa testing areas, respectively. (The Rainier and Shoshone Mesa testing areas are some distance apart, but the testing conditions and seismic coupling in those areas are essentially the same.) The quantitative values of $\log_{10}(Y_e/Y_o)$ are not shown in these figures because most of the explosion yields are classified. The main reason for presenting these figures, less numerical scales for the ordinates, is to show that the ratios of the estimated yields to the official yields are lognormally distributed for each of these testing areas. At the Nevada Test Site, the greatest variation in geological properties is found in Yucca Flat; the standard deviation of $\log_{10}(Y_e/Y_o)$ is somewhat greater for explosions in Yucca Flat than for explosions in the other testing areas. The means of the ratios (Y_e/Y_o) for the explosions in Yucca Flat and Pahute Mesa are approximately unity, as is to be expected because the estimates are based on calibration data for these testing areas.

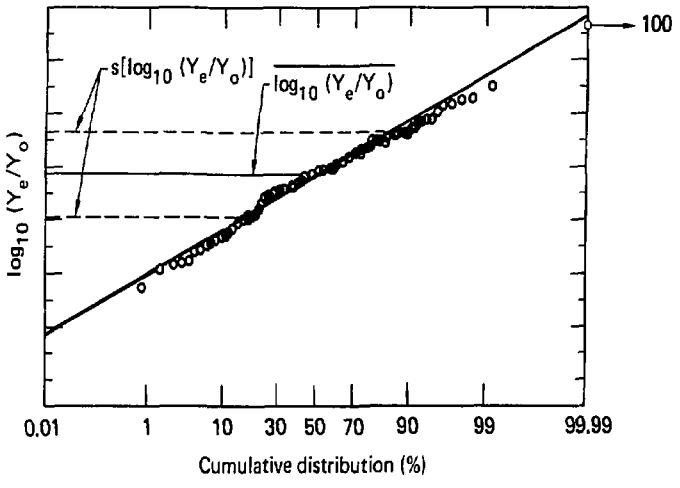

FIG. 37. Cumulative distribution of $\log_{10}(Y_e/Y_o)$ for explosions in Yucca Flat (from Rodean 1979, with Y_e values from Dahlman and Israelson 1977).

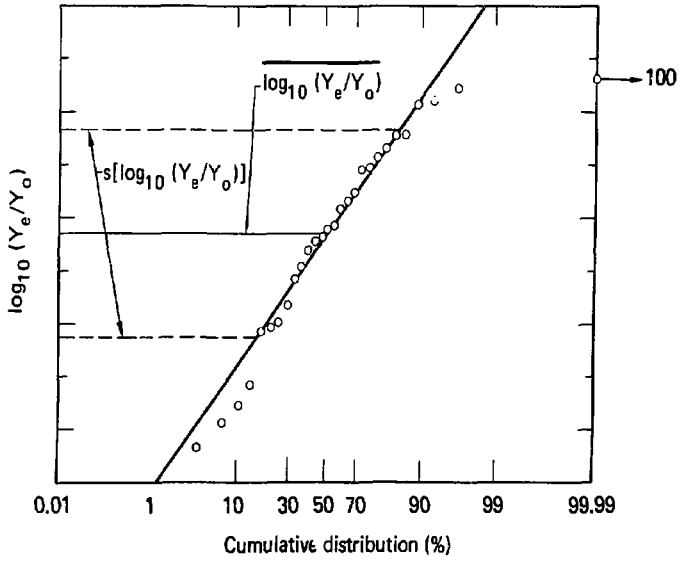

FIG. 38. Cumulative distribution of $\log_{10}(Y_e/Y_o)$ for explosions in Pahute Mesa (from Rodean 1979, with Y_e values from Dahlman and Israelson 1977).

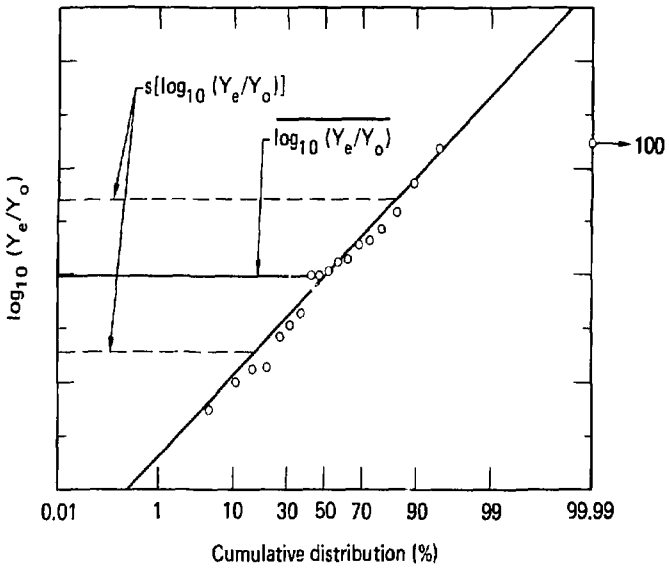

FIG. 39. Cumulative distribution of $\log_{10}(Y_e/Y_o)$ for explosions in Rainier and Shoshone mesas (from Rodean 1971a, with Y_e values from Dahlman and Israelson 1977).

The mean of the ratio (Y_e/Y_o) for Rainier and Shoshone mesas is greater than unity; Dahlman and Israelson did not have any calibration data for these testing areas. As noted by Terhune, Snell, and Rodean (1979), seismic data indicate that the seismic signals from Rainier Mesa are, on the average, a fraction of a magnitude unit greater than those from explosions of comparable yield below the water table in Yucca Flat and Pahute Mesa. This is consistent with the effect of differences in emplacement conditions investigated by Terhune, Snell, and Rodean. (Rainier and Shoshone Mesa explosions generally have greater scaled source radii than explosions in the other testing areas; see Figs. 29 and 30.) However Terhune, Snell, and Rodean concluded that other emplacement and geologic factors that affect signal generation and propagation could be responsible for all or part of the observed seismic magnitude difference.

7. SUMMARY

The phenomena are different, but there are analogies in the early stages of underground chemical and nuclear explosions. At later times, the inelastic processes in the rock are identical in the two types of explosions. There is no known seismic method to

distinguish between chemical and nuclear explosions of comparable yield.

There are three sources of seismic signals from explosions that are coincident in time and space, or nearly so: the explosion itself, explosion-induced tectonic strain release, and (perhaps) surface spall closure or "slapdown." There are also two explosion-related sources of delayed seismic signals: cavity collapse which is coincident in space with the explosion, and aftershocks which may occur several kilometers from the explosion.

Explosions are very inefficient in generating seismic waves; 95 percent or more of the explosion energy is dissipated in inelastic processes in the vicinity of the explosion. Natural variations in shot-point geology can cause differences (for explosions with equal yields) in seismic signal strength of 1 magnitude unit; cavity decoupling can reduce a signal amplitude between 1 and 2 magnitude units. The inelastic stress-wave decay (as a function of the radial coordinate from the center of the explosion) is a strong function of the geological properties of the rock; the observed radial rates of inelastic stress-wave decay are bracketed by simple theoretical relations.

The transition from a nonlinear inelastic stress wave to a linear "elastic" seismic wave is not well defined; in part because ideal elastic stress-wave propagation does not exist in geological media. Assuming spherical symmetry for explosions, the location of the transition is often called the "elastic radius." It is proposed that this transition be defined as the transition between nonlinear inelastic and linear anelastic behavior. Some data indicate that linear anelastic behavior exists in some rocks at strains less than 10^{-6}. More research is needed to define the transition between nonlinear and linear stress-wave response.

The reduced-displacement potential is a convenient approximate fiction. It is a fiction because no real explosion is exactly spherical and ideal elastic stress-wave propagation in rocks does not exist. It is approximate because explosions are approximately spherical and stress-wave propagation can be almost elastic. It is convenient because it is a simple mathematical description of an explosion as a seismic source.

Present programs for the calculation of explosions on large computers are very useful for predicting phenomena in the high-stress zone, but are less useful in accurately predicting seismic-wave radiation from an explosion. This is because the constitutive relations between stress and strain do not model all the processes that are known to occur at low stress levels at which nonlinear inelastic response tends toward linear anelastic response.

In principle, synthetic seismograms can be calculated beginning with the detonation of the explosion and ending with the recording of the seismogram (the forward problem in seismology). However, seismic data can be inverted to obtain only an "equivalent elastic source"; the seismic data cannot be used as inputs to calculate nonlinear inelastic stress-wave propagation backward in space and time (the inverse problem). The reduced-displacement potential is a common solution of the forward and inverse problems. Computer calculations of reduced-displacement potentials for specific explosions indicate that a step function is the principal component of the driving function. Experimental measurements on these explosions indicate the driving function is a step-pulse-impulse function. Seismic data inversion and the matching of synthetic with real seismograms for specific explosions indicate an even greater impulse component in the source function. More research is required to resolve these discrepancies.

A simple spherical explosion model (the reduced-displacement potential) in combination with a theoretical scaling rule (characteristic times and linear dimensions scaled in proportion to the cube-root of explosion yield) is not consistent with observed linear relations between seismic magnitude and the logarithm of the explosion yield. A modified empirical scaling rule in combination with the reduced-displacement potential gives better results for body-wave magnitude vs log yield, but does not account for the observed linear relation between surface-wave magnitude vs log yield. More research is required to better define the effects of yield, depth, and material properties on seismic source parameters. There are speculations and there is some evidence that spall closure or "slapdown" is significant in Rayleigh-wave generation. More research is required to define the role of spall closure in seismic wave generation.

Tectonic strain release makes an explosion appear more "earthquake-like," but apparently not to the extent that the m_b:M_S discriminant between earthquakes and explosions is compromised. The effect on M_S and the Rayleigh wave radiation pattern is significantly different for strike-slip vs dip-slip tectonic release. There are two hypotheses for the release of preexisting tectonic strain by explosions. One is that the strain is released around the weak fractured zone produced by the explosion; a theoretical model has been developed for this phenomenon. The other is that fault motion is triggered near the explosion; a causal theoretical model has not been developed for this phenomenon. Seismic data from many explosions are consistent with both hypotheses, but the large tectonic strain release observed from some explosions is more consistent with the triggering model.

Two final cautions. First, most of the public data (time, yield, depth, medium, etc.) for underground nuclear explosions are

for a limited number of geologic media at one location: alluvium and volcanic rocks (tuff and rhyolite) at the Nevada Test Site. Comparable quantities of data for explosions in other media and at other locations are necessary to provide a balanced perspective and the answers to some important questions. For example, "Are the two m_b vs M_S slopes observed for explosions in Nevada and the USSR a consequence of different slopes for m_b vs log yield relations for the different rocks at these test sites?" Second, the best quality and most complete seismic data we now have for use in seismic discrimination research are from high yield, strongly-coupled explosions. Under a comprehensive test ban, the operational problem will concern low yield, weakly coupled explosions.

8. ACKNOWLEDGMENTS

This lecture summarizes some of my work, but most of it concerns the work of many others who are credited in the references. My colleagues at the Lawrence Livermore National Laboratory, especially F. Followill, D. Larson, P. Moulthrop, and L. Thigpen, made valuable and constructive criticisms of the first draft of this manuscript. Work performed under the auspices of the U.S. Department of Energy by the Lawrence Livermore Laboratory under Contract W-7405-Eng-48.

9. REFERENCES

Ahrens, T. J., and Urtiew, P. A., 1971. The use of shock waves in the vaporization of metals, Lawrence Livermore Laboratory, Report UCRL-51109, Livermore, California.

Aki, K., 1966. Generation and propagation of G waves from the Niigata earthquake of June 16, 1964. Part 2. Estimation of earthquake movement, released energy, and stress - strain drop from the G-wave spectrum, Bull. Earthquake Res. Inst., Tokyo Univ., 44, 73-88.

Aki, K., Bouchon, M., and Reasenberg, P., 1974. Seismic source function for an underground nuclear explosion, Bull. Seism. Soc. Am., 64, 131-148.

Aki, K., Reasenberg, P., DeFazio, T., and Tsai, Y.-B., 1969. Near-field and far-field seismic evidences for triggering of an earthquake by the Benham explosion, Bull. Seism. Soc. Am., 5 [illegible] 2207.

Aki, K., and Tsai, Y.-B., 1972. Mechanism of Love-wave excitation by explosive sources, J. Geophys. Res., 77, 1452-1475.

Archambeau, C. B., 1972. The theory of stress wave radiation from explosions in prestressed media, Geophys. J.R., Astr. Soc., 29, 329-366.

Archambeau, C., and Sammis, C., 1970. Seismic radiation from explosions in prestressed media and the measurement of tectonic stress in the earth, Rev. Geophys., 8, 473-499.

Bakun, W. H., and Johnson, L. R., 1973. The deconvolution of teleseismic P waves from explosions Milrow and Cannikin, Geophys. J. R., Astr. Soc., 34, 321-342.

Basham, P. W., 1969. Canadian magnitudes of earthquakes and nuclear explosions in south-western North America, Geophys. J. R. Astr. Soc., 17, 1-13.

Basham, P. W., and Horner, R. B., 1973. Seismic magnitudes of underground nuclear explosions, Bull. Seism. Soc. Am., 63, 105-131.

Blake, F. G., Jr., 1952. Spherical wave propagation in solid media, J. Acoust. Soc. Am., 24, 211-215.

Boardman, C. R., Rabb, D. D., and McArthur, R. D., 1964. Responses of four rock mediums to contained nuclear explosions, J. Geophys. Res., 69, 3457-3469.

Boucher, G., Ryall, A., and Jones, A. E., 1969. Earthquakes associated with underground nuclear explosions, J. Geophys. Res., 74, 3808-3820.

Brennan, B. J., and Stacey, F. D., 1977. Frequency dependence of elasticity of rock--test of seismic velocity dispersion, Nature, 268, 220-222.

Brune, J. N., and Pomeroy, P. W., 1963. Surface wave radiation patterns for underground nuclear explosions and small-magnitude earthquakes, J. Geophys. Res., 68, 5005-5028.

Burdick, L. J., and Helmberger, D. V., 1979. Time functions appropriate for nuclear explosions, Bull. Seism. Soc. Am., 69, 957-973.

Burton, D. E., and Schatz, J. F., 1975. Rock modeling in TENSOR'74, a two-dimensional Lagrangian shock propagation code, Lawrence Livermore Laboratory, Report UCID-16719, Livermore, California.

Butkovich, T. R., 1967. The gas equation of state for natural materials, Lawrence Radiation Laboratory, Report UCRL-14729, Livermore, California.

Carpenter, E. W., 1967. Teleseismic signals calculated for underground, underwater and atmospheric explosions, Geophysics, 32, 17-32.

Carpenter, E. W., Savill, R. A., and Wright, J. K., 1962. The dependence of seismic signal amplitudes on the size of underground explosions, Geophys. J. R. Astr. Soc., 6, 426-440.

Chabai, A. J., 1965. On scaling dimensions of craters produced by buried explosives, J. Geophys. Res., 70, 5075-5098.

Cherry, J. T., and Petersen, F. L., 1970. Numerical simulation of stress wave propagation from underground nuclear explosions (IAEA-PL-338/15), Peaceful Nuclear Explosions, International Atomic Energy Agency, Vienna.

Chilton, F., Eisler, J. D., and Heubach, H. G., 1966. Dynamics of spalling of the earth's surface caused by underground explosions, J. Geophys. Res., 71, 5911-5919.

Constantino, M. S., 1978. Statistical variation in stress-volumetric strain behavior of Westerly granite, Int. J. Rock Mech. Min. Sci. and Geomech. Abstr., 15, 105-111.

Dahlman, O., and Israelson, H., 1977. Monitoring Underground Nuclear Explosions, Elsevier Scientific Publishing Company, Amsterdam, Ch. 11 and Appendix A.2.5.

Edwards, A. L., and Holzman, R. L., 1968. Thermal effects of a nuclear explosion in salt, the Salmon experiment, Naturwissenschaften, 55, 18-22.

Eisler, J. D., 1967. Near-surface spalling from a nuclear explosion in a salt dome, J. Geophys. Res., 72, 1751-1760.

Eisler, J. D., and Chilton, F., 1964. Spalling of the earth's surface by underground nuclear explosions, J. Geophys. Res., 69, 5285-5293.

Eisler, J. D., Chilton, F., and Sauer, F. M., 1966. Multiple subsurface spalling by underground nuclear explosions, J. Geophys. Res., 71, 3923-3927.

Engdahl, E. R., 1972. Seismic effects of the Milrow and Cannikin nuclear explosions, Bull. Seism. Soc. Am., 62, 1411-1423.

Ericsson, U., 1971. A linear model for the yield dependence of magnitudes measured by a seismographic network, Geophys. J. R. Astr. Soc., 25, 49-69.

Gardner, M. F., and Barnes, J. L., 1942. Transients in Linear Systems, John Wiley and Sons, Inc., New York.

Gauvenet, A., 1970. Experiments with underground nuclear explosions in the Hoggar massif, Proceedings of the American Nuclear Society Topical Meeting, Engineering with Nuclear Explosives, Las Vegas, Nevada, January 14-16, 1970, U.S. Atomic Energy Commission, Washington D.C.

Hamilton, R. M., Smith, B., Fisher, F. G., and Papanek, P. J., 1972. Earthquakes caused by underground nuclear explosions on Pahute Mesa, Nevada Test Site, Bull. Seism. Soc. Am., 62, 1319-1341.

Hanks, T. C., and Wyss, M., 1972. The use of body-wave spectra in the determination of seismic-source parameters, Bull. Seism. Soc. Am., 62, 561-589.

Haskell, N. A., 1967. Analytic approximation for the elastic radiation from a contained underground explosion, J. Geophys. Res., 72, 2583-2587.

Heckman, R. A., 1964. Deposition of thermal energy by nuclear explosives, Lawrence Radiation Laboratory, Report UCRL-7801, Livermore, California.

Helmberger, D. V., and Harkrider, D. G., 1972. Seismic source descriptions of underground explosions and a depth discriminant, Geophys. J. R. Astr. Soc., 31, 45-66.

Herbst, R. F., Werth, G. C., and Springer, D. L., 1961. Use of large cavities to reduce seismic waves from underground explosions, J. Geophys. Res., 66, 959-978.

Hirasawa, T., 1971. Radiation patterns of S waves from underground nuclear explosions, J. Geophys. Res., 76, 6440-6454.

Holzer, F., 1966. Calculation of seismic source mechanisms, Proc. Roy. Soc., London, Ser. A, 290, 408-429.

Hudson, J. A., and Douglas, A., 1975. Rayleigh wave spectra and group velocity minima, and the resonance of P waves in layered structures, Geophys. J. R. Astr. Soc., 42, 175-188.

Israelson, H., Slunga, R., and Dahlman, O., 1974. Aftershocks caused by the Novaya Zemlya explosion on October 27, 1973, Nature, 247, 450-452.

Jaeger, J. C., and Cook, N. G. W., 1971. Fundamentals of Rock Mechanics, Science Paperbacks, London.

Jeffreys, H., 1931. On the cause of osillatory movement in seismograms, Mon. Notic. Roy. Astron. Soc., Geophys. Suppl., 2, 407-416.

Johansson, C. H., and Persson, P. A., 1970. Detonics of High Explosives, Academic Press, Inc., New York.

Johnson, G. W., Higgins, G., and Violet, C., 1959. Underground nuclear detonations. J. Geophys. Res., 64, 1457-1470.

Kawasumi, H., and Yosiyama, R., 1935. On an elastic wave animated by the potential energy of initial strain, Bull. Earthquake Res. Inst., Tokyo Univ., 13, 496-503.

Kedrovskii, O. L., 1970. Primenenie kamufletnyk yadernykh vzryvov v promyshlennost. (IAEA-PL-388/20), Peaceful Nuclear Explosions, International Atomic Energy Agency, Vienna.

Knopoff, L.,and MacDonald, G. J. F., 1958. Attenuation of small amplitude stress waves in solids, Rev. Mod. Phys., 30, 1178-1192.

Lambert, D. G., Flinn, E. A., and Archambeau, C. B., 1972. A comparative study of the elastic wave radiation from earthquakes and underground explosions, Geophys. J. R. Astr. Soc., 29, 403-432.

Larson, D. B., 1977a. The relationship of rock properties to explosive energy coupling, Lawrence Livermore Laboratory, Report UCRL-52204, Livermore, California.

Larson, D. B., 1977b. Lawrence Livermore Laboratory, Livermore, California, private communication.

Larson, D. B., 1980a. Shock wave studies in Blair dolomite, J. Geophys. Res., 85, 293-297.

Larson, D. B., 1980b. Lawrence Livermore Laboratory, Livermore, California, private communication.

Larson, D. B., and Anderson, G. D., 1979a. Plane shock wave studies of porous geological media, J. Geophys. Res., 84, 4592-4600.

Larson, D. B., and Anderson, G. D., 1979b. Plane shock wave studies of Westerly granite and Nugget sandstone, Lawrence Livermore Laboratory, Report UCRL-82264, accepted for publication in Int. J. Rock Mech. Min. Sci. and Geomech. Abstr.

Latter, A. L., LeLevier, R. E., Martinelli, E. A., and McMillan, W. G., 1961. A method of concealing underground nuclear explosions, J. Geophys. Res., 66, 943-946.

Liebermann, R. C., and Pomeroy, P. W., 1969. Relative excitation of earthquakes and underground explosions, J. Geophys. Res., 74, 1575-1590.

Maenchen, G., and Sack, S., 1964. The tensor code, Methods in Computational Physics, Vol. 3, Academic Press, Inc., New York.

Marshall, P. D., 1979. AWRE, Blacknest, England, private communication.

Marshall, P. D., and Basham, P. W., 1972. Discrimination between earthquakes and underground explosions employing an improved M_S scale, J. Geophys. Res., 28, 431-458.

Marshall, P. D., Douglas, A., and Hudson, J. A., 1971. Surface waves from underground explosions, Nature, 234, 8-9.

Marshall, P. D., Springer, D. L., and Rodean, H. C., 1979. Magnitude corrections for attenuation in the upper mantle, Geophys. J. R. Astr. Soc., 57, 609-638.

McEvilly, T. V., and Peppin, W. A., 1972. Source characteristics of earthquakes, explosions, and afterevents, Geophys. J. R. Astr. Soc., 31, 67-82.

Meyer, M. L., 1964. On spherical near fields and far fields in elastic and visco-elastic solids, J. Mech. Phys. Solids, 12, 77-111.

Michaud, L., 1968. Explosions nuclaires souterraines etude des rayone de cavity, Commissariat A L'Energie Atomique, Rapport CEA-R-3594.

Mueller, R. A., 1969. Seismic energy efficiency of underground nuclear detonations, Bull. Seism. Soc. Am., 59, 2311-2323.

Mueller, R. A., and Murphy, J. R., 1971. Seismic characteristics of underground nuclear detonations. Part I. Seismic spectrum scaling, Bull. Seism. Soc. Am., 61, 1675-1692.

Müller, G., 1969. Theoretical seismographs for types of point-sources in layered media. Part III. Single force and dipole sources of arbitrary orientation, J. Geophys., 35, 347-371.

Müller, G., 1973. Seismic moment and long-period radiation of underground nuclear explosions, Bull. Seism. Soc. Am., 63, 847-857.

Murphey, B. F., 1961. Particle motion near explosion in Halite, J. Geophys. Res, 66, 947-958.

Murphy, J. R., 1977. Seismic source functions and magnitude determinations for underground nuclear detonations, Bull. Seism. Soc. Am., 67, 135-158.

Patterson, D. W., 1966. Nuclear decoupling, full and partial, J. Geophys. Res., 71, 3427-3426.

Patton, H. J., 1980. Lawrence Livermore Laboratory, Livermore, California, private communication.

Peppin, W. A., 1977. A near-regional explosion source model for tuff, Geophys. J. R. Astr. Soc., 48, 331-349.

Perret, W. R., 1972a. Gasbuggy seismic source measurements, Geophysics, 47, 301-312.

Perret, W. R., 1972b. Seismic-source energies of underground nuclear explosions, Bull. Seism. Soc. Am., 62, 763-774.

Press, F., and Archambeau, C., 1962. Release of tectonic strain by underground nuclear explosions, J. Geophys. Res., 67, 337-343.

Randall, M. J., 1973. The spectral theory of seismic sources, Bull. Seism. Soc. Am., 63, 1133-1144.

Rawson, D. E., 1963. Review and a summary of some Project Gnome results, Trans. Amer. Geophysics Union, 44, 129.

Rawson, D. E., Taylor, R. W., and Springer, D. L., 1967. A review of the Salmon Experiment, a nuclear explosion in salt, Naturwissenschaften, 54, 525-531.

Ringdahl, F., 1976. Maximum-likelihood estimation of seismic magnitude, Bull. Seism. Soc. Am., 66, 789-802.

Rodean, H. C., 1971a. Nuclear-Explosion Seismology, U.S. Atomic Energy Commission.

Rodean, H. C., 1971b. Cavity decoupling of nuclear explosions, Lawrence Livermore Laboratory, Report UCRL-51097, Livermore, California.

Rodean, H. C., 1972. An energy approach to seismic coupling analysis, J. Geophys. Res., 77, 3129-3145.

Rodean, H. C., 1979. Statistical analysis of Swedish yield estimates for U.S. underground nuclear explosions, Lawrence Livermore Laboratory, Report UCRL-52698, Livermore, California. (Title U, Report-Confidential FRD).

Rogers, L. A., 1966. Free-field motion near a nuclear explosion in salt: Project Salmon, J. Geophys. Res., 71, 3145-3426.

Rygg, E., 1979. Anomalous surface waves from underground explosions, Bull. Seism. Soc. Am., 69, 1995-2002.

Savage, J. C., and Hasegawa, H. S., 1967. Evidence for a linear attenuation mechanism, Geophysics, 32, 1003-1014.

Schatz, J. F., 1973. The physics of SOC and TENSOR, Lawrence Livermore Laboratory, Report UCRL-51352, Livermore, California.

Schatz, J. F., 1974. SOC73, a one-dimensional wave propagation code for rock media, Lawrence Livermore Laboratory, Report UCRL-51639, Livermore, California.

Schatz, J., Kusubov, A., Hearst, J., Abey, A., Snell, C., and Thigpen, L., 1977. Rock mechanic project progress and results: rock fracture and pore collapse, Lawrence Livermore Laboratory, Report UCID - 17527, Livermore, California.

Sedov, L. I., 1959. Similarity and Dimensional Methods in Mechanics, 4th Ed., Academic Press, Inc., New York, pp.210-238.

Selberg, H. L., 1952, Transient compressional waves from spherical and cylindrical cavities, Ark. Phys., 5, 97-108.

Smith, S. W., 1963. Generation of seismic waves by underground explosions and the collapse of cavities, J. Geophys. Res., 68, 1447-1483.

Springer, D. L., 1974. Secondary sources of seismic waves from underground nuclear explosions, Bull. Seism. Soc. Am., 64, 581-594.

Springer, D. L., and Denny, M. D., 1976. Seismic spectra of events at regional distances, Lawrence Livermore Laboratory, Report UCRL-52048, Livermore, California.

Springer, D. L., Denny, M. D., Healy, J., and Mickey, W., 1968. The Sterling experiment: decoupling of seismic waves by a shot-generated cavity, J. Geophys. Res., 73, 5995-6011.

Springer, D. L., and Hannon, W. J., 1973. Amplitude-yield scaling for underground nuclear explosions, Bull. Seism. Soc. Am., 63, 477-500.

Springer, D. L., and Kinnaman, R. L., 1971. Seismic source summary for U.S. nuclear underground explosions, 1961-1970, Bull. Seism. Soc. Am., 61, 1073-1098.

Springer, D. L., and Kinnaman, R. L., 1975. Seismic source summary for U.S. nuclear underground explosions, 1971-1973, Bull. Seism. Soc. Am., 65, 343-349.

Taylor, G., 1950a. The formation of a blast wave by a very intense explosion. I. Theoretical discussion. Proc. Roy. Soc. London, Series A, 201, 159-174.

Taylor, G., 1950b. The formation of a blast wave by a very intense explosion. II. The atomic explosion of 1945. Proc. Roy. Soc. London, Series A, 201, 175-186.

Terhune, R, W., Glenn, H. D., Burton, D. E., and Rambo, J. T., 1977a. Containment analysis for the simultaneous detonation of two nuclear explosions, Lawrence Livermore Laboratory, Report UCRL-52268, Livermore, California.

Terhune, R, W., Glenn, H. D., Burton, D. E., and Rambo, J. T., 1977b. Calculational examination of the Baneberry event, Lawrence Livermore Laboratory, Report UCRL-52365, Livermore, California.

Terhune, R. W., Snell, C. M., and Rodean, H. C., 1979. Enhanced coupling and decoupling of underground nuclear explosions, Lawrence Livermore Laboratory, Report UCRL-52806, Livermore, California.

Toksöz, M. N., Ben-Menahem, A., and Harkrider, D. G., 1964. Determination of source parameters of explosions and earthquakes by amplitude equalization of seismic surface waves. 1. Underground nuclear explosions, J. Geophys. Res., 69, 4355-4366.

Toksöz, M. N., Ben-Menahem, A., and Harkrider, D. G., 1965. Determination of source parameters of explosions and eathquakes by amplitude equalization of seismic surface waves. 2. Release of tectonic strain by underground nuclear explosions and mechanisms of earthquakes, J. Geophys. Res., 70, 907-922.

Toksöz, M. N., and Kehrer, H. H., 1972. Tectonic strain release by underground nuclear explosions and its effect on seismic discrimination Geophys. J. R. Astr. Soc., 31, 141-161.

Toman, J., Sisemore, C., and Terhune, R., 1973. The Rio Blanco experiment: subsurface and surface effects and measurements, Lawrence Livermore Laboratory, Report UCRL-51504, Livermore, California.

Trulio, J., 1977. Applied Theory Inc., Los Angeles, private communication.

Trulio, J., 1979. Applied Theory Inc., Los Angeles, private communication.

Tsai, Y.-B., and Aki, K., 1971. Amplitude spectra of surface waves from small earthquakes and underground nuclear explosions, J. Geophys. Res., 76, 3940-3952.

Viecelli, J. A., 1973a. The linear Q and the calculation of decaying spherical shocks in solids. J. Comp. Phys., 12, 187-201.

Viecelli, J. A., 1973b. Spallation and the generation of surface waves by an underground explosion, J. Geophys. Res., 78, 2475-2487.

von Neumann, J., 1963. Collected works, Vol. VI, Pergamon Press, Oxford, pp 219-237.

von Neumann, J., and Richtmyer, R. D., 1950. A method for the numerical calculation of hydrodynamic shocks, J. Appl. Phys., 21, 232-237.

von Seggern, D., and Blandford, R., 1972. Source time functions and spectra for underground nuclear explosions, Geophys. J. R. Astr. Soc., 31, 83-97.

Werth, G. C., and Herbst, R. F., 1963. Comparison of amplitude of seismic waves from nuclear explosions in four mediums, J. Geophys. Res., 68, 1463-1475.

Werth, G. C., Herbst, R. F., and Springer, D. L., 1962. Amplitude of seismic arrivals from the M discontinuity, J. Geophys. Res., 67, 1587-1610.

Wheeler, V. E., Preston, R. G., and Frerking, C. E., 1976. Trapped stress waves in underground nuclear explosions, Lawrence Livermore Laboratory, Report UCRL-52012, Livermore, California. (Title-U, Report-Confidential FRD).

Wilkins, M. L., 1964. Calculation of elastic-plastic flow, in Methods in Computational Physics, Vol. 3, Academic Press, Inc. New York.

Winkler, K., Nur, A., and Gladwin, M., 1979. Friction and seismic attenuation in rocks, Nature, 277, 528-531.

Yoshiyama, R., 1963. Note on earthquake energy, Bull. Earthquake Res. Inst. Tokyo Univ., 41, 687-697.

Zel'dovich, Ya. B., and Raizer, Yu. P., 1966. Physics of Shock Waves and High-Temperature Hydrodynamic Phenomena, Vol. 1, Academic Press, Inc., New York.

Zel'dovich, Ya. B., and Raizer, Yu. P., 1967. Physics of Shock Waves and High-Temperature Hydrodynamic Phenomena, Vol. 2, Academic Press, Inc., New York.

CONTENTS